DOI: 10.1002/ejic.200900761

Grids with Unusual, High Nuclearity – A Structural Approach

Adrian-Mihail Stadler*[a,b]

Dedicated to Professor Jean-Marie Lehn on the occasion of his 70th birthday

Keywords: Grid-like complexes / High-nuclearity complexes / Supramolecular chemistry / Self-assembly / Coordination chemistry

Polynuclear supramolecular homoleptic grid-like architectures containing s^2 (s = 3, 4, 5) metal ions arranged like the elements of a square matrix and located in the coordination spheres generated at the intersection points ("nodes") of the 2s bridging s-topic ligands (the "bars" of the grid), are quite rare, but they are fascinating by their formation by self-assembly, their structures and properties. Moreover, heteroleptic hexanuclear complete [2×3] grids, as well as other kinds of grids containing more than four metal centres were reported. The access to such grids necessitates the design of appropriate polytopic ligands. However, in several cases, incomplete grids were obtained instead of the expected complete grids. The structural diversity of the grids with unusual, high nuclearity reported until now is herein reviewed.

The introductory section of this review will be followed by the presentation of the structural principles governing these grids, of their typology, of the means of characterization and by a section on coordination-induced conformational and shape changes of the ligands.

1. Introduction

Essential, major contributions to the field of high-nuclearity grids were provided by the groups of Professors *Jean-Marie Lehn* (Strasbourg, France), who initiated this field of research by reporting the first Ag_9 nonanuclear grid in 1994 (see ref.[16a]) and the first Pb_{16} hexadecanuclear one in 1999 (see ref.[17]) and further reported various types of high-nuclearity grids, and *Laurence K. Thompson* (St. John's, Canada), who initiated and developed the field of high-nuclearity grids (M_9–M_{25}) generated by bis- and poly-acyl-hydrazone-type ligands (see, for example, ref.[3a(1),3a(3–5)]) and recently reported the first heterometallic nonanuclear grids (see ref.[29,47]), as well as numerous other complete and incomplete grids herein reviewed (vide infra). The heteroleptic hexanuclear grids reported until now are due to Professors *Jean-Marie Lehn* (see ref.[37a]) and *Michael Schmittel* (see ref.[37c]) (Siegen, Germany). Relevant work on high-nuclearity grids was also done by the groups of Professors *Craig J. Matthews* (see ref.[32,38]), *Chunying Duan* and *Qingjin Meng* (see ref.[11]).

After a short presentation of the interest for grids and squares, the meaning of the term "grid with unusual, high nuclearity" for the purpose of this review will be stated, and some aspects that make such grids so attractive will be mentioned.

[a] Institut de Science et d'Ingénierie Supramoléculaires, Université de Strasbourg,
8 allée Gaspard Monge, Strasbourg 67083, France
[b] Karlsruhe Institute of Technology (KIT), Forschungszentrum Karlsruhe (FZK), Institute for Nanotechnology (INT),
Postfach 3640, 76021 Karlsruhe, Germany
E-mail: mstadler@isis.u-strasbg.fr
Supporting information for this article is available on the WWW under http://dx.doi.org/10.1002/ejic.200900761.

Adrian-Mihail Stadler, recipient of awards at several Chemistry Olympiads, studied chemistry at the Universities of Bucharest, Paris XI – Orsay and Strasbourg, and law at the Universities of Paris I Panthéon – Sorbonne and Strasbourg. He received his Ph.D. degree in chemistry (2004) under the supervision of Professor Jean-Marie Lehn, in Strasbourg. For his Ph.D. research, he was awarded the Sigma–Aldrich Prize of the Société Française de Chimie and a Université Louis Pasteur Prize. He participated as a postdoctoral researcher in the European Project AMNA. His current research interests are coordination and supramolecular chemistry.

1.1. Fascinating Grids and Squares

The field of supramolecular architectures[1] with defined and programmed shapes has become very large, and its evolution has increasing velocity. Among them, square-like[2] and grid-like[3a] supramolecular architectures, which are examples of self-organization by design,[4] have been studied intensively. Particular interest is manifested for the properties and potential applications of such architectures in the field of information storage or magnetic materials.[5] Metal centres of such metallo-supramolecular assemblies may be addressed by scanning tunnelling spectroscopy (STS), current induced tunnelling spectroscopy (CITS).[6] The square motif was used to conceive bioactive molecules, for example, the recently reported self-assembled platinum square that acts as an efficient G-quadruplex binder and telomerase inhibitor[7a] or synthetic analogues, such as the "artificial enzymes" formed through directed assembly of molecular square encapsulated epoxidation catalysts.[7b] From a functional point of view that concerns the transport of small species, a remarkable feature of several [2 × 2] grids is their aptitude to encapsulate anions.[8]

Square-like and grid-like motifs are also interesting for crystal engineering;[9] however, such solid-state polymeric squares or grids dissociate partially or totally in solution, in contrast with discrete grid-like or square-like architectures that can generally be observed in solution.

1.2. Delimitation of the Subject Matter

As the word "grid" may be used with several meanings in the field of supramolecular architectures, for the purpose of this review, "grid" means a metallo-supramolecular architecture in which ligands and metal ions form a rectangular or square array and in which ligands that form nodes (the metal ion and its coordination sphere) *are crossed*, they intersect as in a cross (Figure 1a). The projections of the two concerned ligands on a plane orthogonal to their planes should intersect. Square-like bidimensional architectures, in which the ligands are perpendicular *but not crossed*[9b,9c] (Figure 1b), in spite of being very interesting, are not reviewed herein.

The "smallest" type of grid that may exist is the [2 × 2] one and it contains four metal ions, already a complex with high nuclearity. Despite the recent progress, grids that have more than four metal centres are quite uncommon or unusual with respect to [2 × 2] grids, which are more frequently reported. Thus, for the purpose of this review, "grid with unusual, high nuclearity" means a grid that is more than tetranuclear.

1.3. Interest for Grids with "Unusual, High" Nuclearity

There are several features that make grids with unusual, high nuclearity interesting:

– most of these grids are highly charged cations, and their charge may reach +32;

– they are the result of a strong process of self-organization, as numerous ligands and metal ions (for example, for a hexadecanuclear complete grid, 16 metal ions and 8 ligands) are involved in their selective formation;

– they have nanometric sizes, the volume of the smallest rectangular cuboid that may contain, for example, the [4 × 4] Pb^{II} grid generated by tetratopic ligand **11** being about 20000 $Å^3$;

– their largest faces can be seen as nanoplatforms (often positively charged) having a surface of, for example, about 1000 $Å^2$ for a [4 × 4] Pb^{II} grid generated by tetratopic ligands **11** and **12** (vide infra);

– within the grid, the positions of the metal ions are precisely known; such a set of metal ions is obtained just by self-assembly, without nanotechnological intervention, thus their formation belongs to the field of chemionics;[4d]

– magnetic exchange interactions were observed within grids incorporating paramagnetic metal ions (see, for example, ref.[5]);

– those grids that display antiferromagnetic exchange interactions might find potential applications as building blocks for quantum computers;[10]

– most grids with high nuclearity can also be seen as two-dimensional oligomers or polymers;[3b]

– they are quite rare, uncommon architectures.

2. General Structural Principles of Grids with Unusual, High Nuclearity

2.1. Metal Ions and Ligands

Most part of grids with unusual, high nuclearity reported until now contain one kind of polytopic ligand L (homoleptic grids) and one kind of metal ion M (homometallic grids). Sometimes, one or more supplementary ligands L′ may coordinate the metal ion or replace the initial ligands. A number, u, of counterions insure the electric neutrality of the complex. The general formula of such a $[m \times n]$ grid is $[M_r L_{m+n}(L')_t]X_u$, where $r \leq m \times n$.

Grids are based on the capacity of metal ions to act as coordination node inductors, on binding to the appropriate coordination sites of ligands. Depending on the nature of the metal ion and of the ligand, a grid-node may be a metal ion and two bidentate (Figure 1e) or tridentate (Figure 1c) coordination sites from two different ligands. Less com-

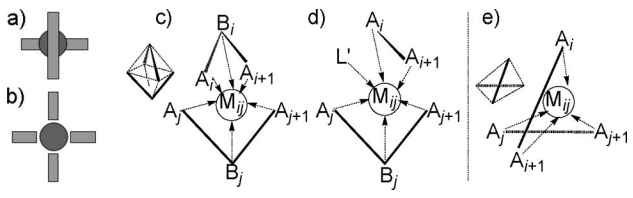

Figure 1. Representation of a cross-node (a) from a grid-like complex and of an uncross-node (b) from a square-like complex. A grid-node, i.e. the metal ion and its coordination sphere: (c) octahedral coordination $[(A_iB_iA_{i+1})M_{ij}(A_jB_jA_{j+1})]$ (vide infra Figure 4a–f); (d) octahedral coordination $[(A_iB_iA_{i+1})M_{ij}(A_jA_{j+1})(L')]$; (e) tetrahedral coordination $[(A_iA_{i+1})M_{ij}(A_jA_{j+1})]$.

monly, other combinations, such as a metal ion, a tridentate coordination site, a bidentate ligand and a supplementary ligand (Figure 1d), or a metal ion, a tridentate coordination site and a bidentate ligand etc., as well as metal centres with coordination number greater than six were found.

From a formal point of view, a bidentate site can be shown as A_i-A_{i+1}, each unit, A_i and A_{i+1}, providing a donor atom. A tridentate site can be shown as A_i-B_i-A_{i+1}, where B_i is a unit providing a donor atom. The main types of tri- and bidentate sites from ligands and complexes discussed

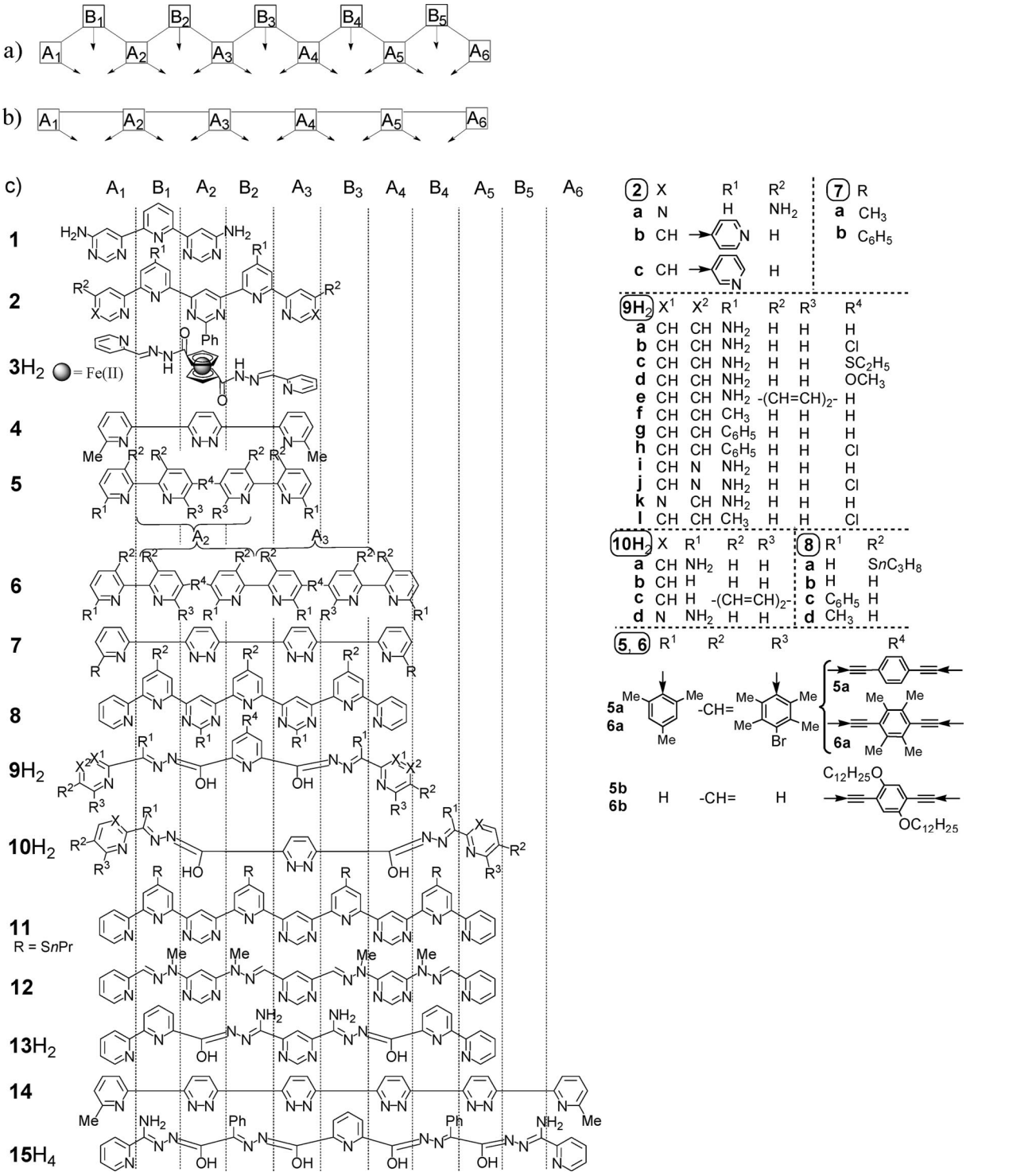

Figure 2. Representation of a ligand that has six tridentate (a) or six bidentate (b) sites; (c) classes of ligands that generated the high-nuclearity grids defining the focus of this review, represented in the conformation they usually adopt in grids. Ligands **9**H_2, **10**H_2, **13**H_2 and **15**H_4 are represented as their "enolic" form.

herein are shown in Figure 4(1) to (10). A ligand with s bidentate coordination sites may be shown as A_1-A_2-...-A_s-A_{s+1} (Figure 2b), while a ligand with s tridentate coordination sites may be shown as A_1-B_1-A_2-B_2-...-A_s-B_s-A_{s+1} (Figure 2a). There are also ligands having tridentate as well as bidentate sites, such as A_1-B_1-A_2-A_3-A_4-B_4-A_5 (e.g. **10**H_2) that have two terminal tridentate (A_1-B_1-A_2, A_4-B_4-A_5) and two internal bidentate (A_2-A_3, A_3-A_4) sites.

All ligands that generated high-nuclearity grids reported until now are symmetric. The condition of symmetry is: where $1 \leq i,j \leq s + 1$ and $i - 1 = s + 1 - j$, then $A_i = A_j$ and $B_i = B_j$ (identity of each two units equidistant from the ends).

In several cases (see Figure 23), a grid generated by an s-site ligand may be described by means of a $[t \times t]$ matrix, where $t > s$ or $t < s$.

The complete grid generated by an s-tridentate-site-ligand has s^2 octahedral coordination spheres, and the one generated by an s-bidentate-site-ligand has s^2 tetrahedral coordination spheres. However, in the case of a symmetric "mixed-site" s-topic ligand incorporating b bidentate sites and t tridentate sites ($b + t = s$), the $[s \times s]$ grid has b^2 tetrahedral coordination spheres, t^2 octahedral ones and $2bt$ pentacoordinate-geometry ones. Thus, the $[4 \times 4]$ grid generated by **10**H_2 will present four octahedral (corners), four tetrahedral (centre) and eight pentacoordinate-geometry spheres (sides). To assemble a homometallic homovalent grid of this type, a metal ion that can adopt all these types of coordination geometry is required (and the size of the metal ion is also a problem, because these coordination spheres require cations of different size). Otherwise, the probability of obtaining an incomplete grid or another kind of architecture is very high. This problem could also be solved: (i) by choosing an appropriate mixture of metal ions whose geometry match the coordination requirements above, thus generating a heterometallic grid, or (ii) by using an octahedral metal ion together with supplementary small ligands (like solvent molecules bearing donor atoms) that may fit into the grid and complete the tetra- and pentacoordinate geometry spheres to reach hexacoordinate geometry.

The design of grid-generating ligands as sequences of bi- and tridentate coordination sites arranged in the appropriate fashion means incorporating into the ligand the coordinative information that will induce the self-assembly process on "reading" by the appropriate metal ions that may bind to such sites in a ratio of one metal ion to two sites. Several factors (solvent, anion) may induce another fashion of "reading" this structural information, and, in several cases, incomplete grids or other kinds of architectures may form.[3a(5)]

2.2. General Matrix-Like Representation of Grids

The general formula of a typical complete grid-like cation generated by $2s$ molecules of neutral ligand containing s tridentate coordination sites A_1-B_1-A_2-B_2-...-A_s-B_s-A_{s+1} with s^2 octahedral metal ions M^{f+} is $[M_s^2(A_1\text{-}B_1\text{-}A_2\text{-}B_2\text{-}...\text{-}A_s\text{-}B_s\text{-}A_{s+1})_{2s}]^{fs2+}$. It can ideally be represented as a matrix (Figure 3) whose elements are cross-nodes of general formula $[(A_iB_iA_{i+1})M_{ij}(A_jB_jA_{j+1})]$ (Figure 1c; see also Figure 4a–f) for an octahedral metal ion M, and $[(A_iA_{i+1})M_{ij}(A_jA_{j+1})]$ for a tetrahedral one (Figure 1e). In this matrix-like representation, L_Ri represents the ligand that corresponds to row i, and L_Cj represents the ligand that corresponds to column j. The subscript i from M_{ij} corresponds to the row L_Ri, i.e. to the site i of the column L_Cj; conversely, the subscript j corresponds to the column L_Cj, i.e. to the site j of the row L_Ri.

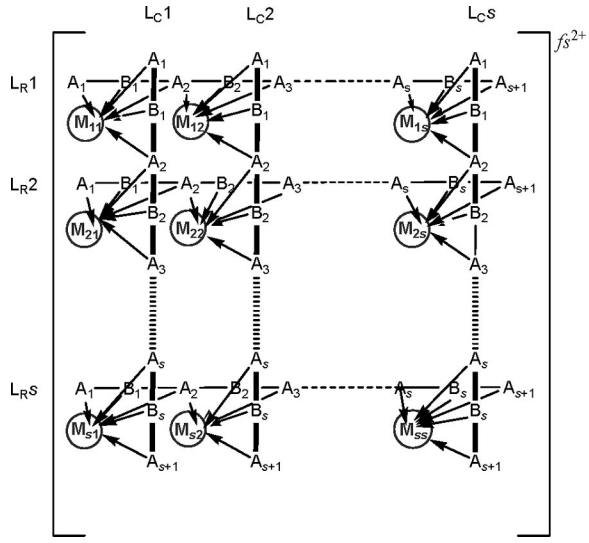

Figure 3. Matrix-like representation of a complete $[s \times s]$ grid-like complex of general formula $[M_s^2(A_1\text{-}B_1\text{-}A_2\text{-}B_2\text{-}...\text{-}A_s\text{-}B_s\text{-}A_{s+1})_{2s}]^{fs2+}$. In this example the coordination geometry of cations M_{ij} ($1 \leq i,j \leq s$) is octahedral.

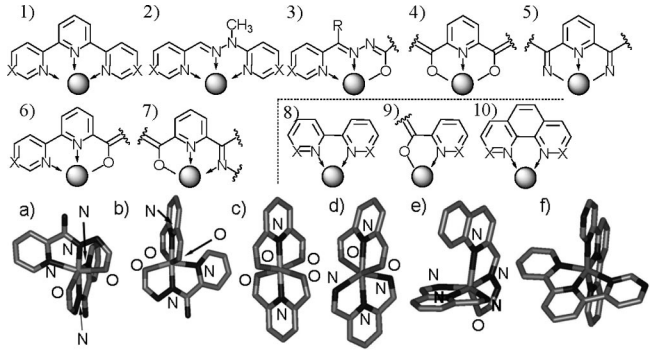

Figure 4. Types of tri- (1–7) and bidentate (8–10) coordination sites (X = CH or N) of ligands and complexes discussed herein. Various types of octahedral arrangements of donor atoms found in the complexes discussed herein: (a) *cis*-N_2O_4, (b) *mer*-N_3O_3, (c) *trans*-N_2O_4 in grid $[Cu^{II}_9(\mathbf{9a}H)_6](NO_3)_{12}\cdot 9H_2O$; (d) *trans*-$N_4O_2$, (e) N_5O in grid $[Mn^{II}_9(\mathbf{9e})_6](ClO_4)_6\cdot 8H_2O$; (f) N_6 in grid $[Fe_4(\mathbf{2b})_4]^{8+}$.

This matrix-like representation, together with the representation of the ligands as sequences of coordinating units connected between them, is also a way to emphasize the importance of the structural design required in order to obtain grids with high nuclearity. This formalism is a means to rationalize and facilitate the conception of ligands and the choice of coordinating units. However, it should be

noted that the formation of the predicted grid-like metallosupramolecular architecture might not be the unique self-assembly pathway of the metal ion/ligand system, and, even with the suitable metal ion and ligand, other architectures may form instead of the expected grid.

One could wonder how to choose the matrix, how to number its metal centres and ligands. For example, in a grid in which one ligand is missing, would this ligand be a row or a column? As the matrix-like representation is not an absolute system, but a relative one, both solutions are correct. In the presentation of structural aspects of grids, reference will often be made to the matrix-like representation, but it will not be represented in each case.

The most common atoms or groups of atoms that separate the metal centres (M) are O (M,O,M sequences), N,N (in pyridazine rings; M,N,N,M sequences) and N,C,N (in pyrimidine rings; M,N,C,N,M sequences). They belong to A_i units, where $2 \leq i \leq s$.

The connexion between the units A_i and B_i, B_i and A_{i+1}, or A_i and A_{i+1}, is usually a simple bond that allows rotation of the units in the free ligands; in some cases, this connection is rigid, like the –CH=CH– bridge found in phenanthroline. Most of the units A_i and B_i are rigid, being heterocycles, but in several cases they are flexible (hydrazones, ferrocenes, acetylene derivatives). Generally, A_1 and A_{s+1} are py_1 (2-substituted pyridine) rings, and B_i is py_2 (2,6-disubstituted pyridine) or hyz (hydrazone –CH=N–NH–) group (see Figure 2c).

2.3. Anionic Ligands

If the ligand is anionic, of charge d^-, then the above general formula becomes $[M_s^2(A_1\text{-}B_1\text{-}A_2\text{-}B_2\text{-}...\text{-}A_s\text{-}B_s\text{-}A_{s+1})_{2s}]^{(fs2-2ds)+}$. Within the field of grids with high nuclearity reported until now, this situation currently appears with ligands that contain acylhydrazone[20a] fragments, $R^1R^2C{=}N{-}NH{-}CO{-}R^3$, where the acidic –NH– group or the –OH group of the corresponding tautomer, $R^1R^2C{=}N{-}N{=}C(OH){-}R^3$, can be deprotonated (Scheme 1). This may happen spontaneously during grid formation or upon addition of base. It was found (vide infra) that both N and O atoms can act as donors. Within the field of [2 × 2] grids, other –NH– groups that can be deprotonated are those of hydrazones[20b] and amides.[20c]

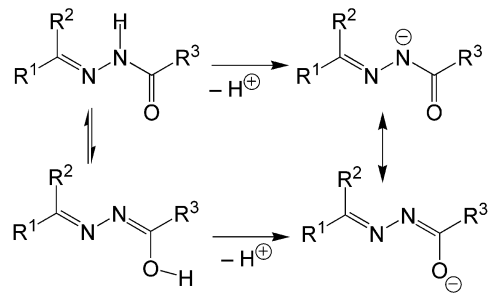

Scheme 1. Deprotonation of the –NH– group of an acylhydrazone.

2.4. Types of High Nuclearity

One can distinguish between "internal" and "external" high nuclearity.

2.4.1. Internal High Nuclearity

Classically, the high nuclearity is reached by increasing the number of coordination sites of the ligand, which should be greater than two. Thus, the nuclearity of the complete grid obtained with this ligand will be greater than four.

High nuclearity may also be attained by another strategy (different from increasing the number of sites of the bridging ligand), which is the incorporation of a unit containing a metal ion into a 2-site ligand that usually forms a [2 × 2] grid.

In both of the above cases, the high nuclearity is internal, located inside the perimeter delimited by the ligands that form the grid.

2.4.2. External High Nuclearity

There can also be grids that have several supplementary sites that bind metal ions or link the grids between them (as in polymeric grids that can be seen as extended supramolecular grids), the said sites being located outside the perimeter delimited by the ligands that form the grid. In such cases, the high nuclearity is external (vide infra).

3. Structural Typology of Grids with Unusual, High Nuclearity

There are two main classes: complete and incomplete grids.

3.1. Complete Grids

A complete grid generated by an *s*-site ligand (an *s*-topic ligand) is an [*s* × *s*] grid in which all coordination nodes are occupied by metal ions, all 2*s* expected ligands and all s^2 metal ions being present. Within the class of complete grids there are: "internally" extended [2 × 2] grids, polymeric complete grids and classical complete [*s* × *s*] grids ($5 \geq s \geq 3$).

3.1.1. "Internally" Extended Complete [2 × 2] Grids

The high nuclearity is reached by incorporating units containing metal centres into ligands that generate [2 × 2] grids. Ligand $\mathbf{3}H_2$ has a ferrocene unit between two hydrazidopyridine fragments (Figure 2c). The complex $[Ni_4(\mathbf{3})_4]$ (Figure 5a,b), obtained by reaction of ligand **3** with 1 equiv. of $Ni(BF_4)_2$ and 2 equiv. of NaOH in methanol, is an octanuclear grid that contains 4 Fe^{II} and 4 Ni^{II}.[11] In two of the four ligands of the extended grid $[Ni_4(\mathbf{3})_4]$, the tridentate sites are *anti* oriented, while in the other two they are *syn* oriented.

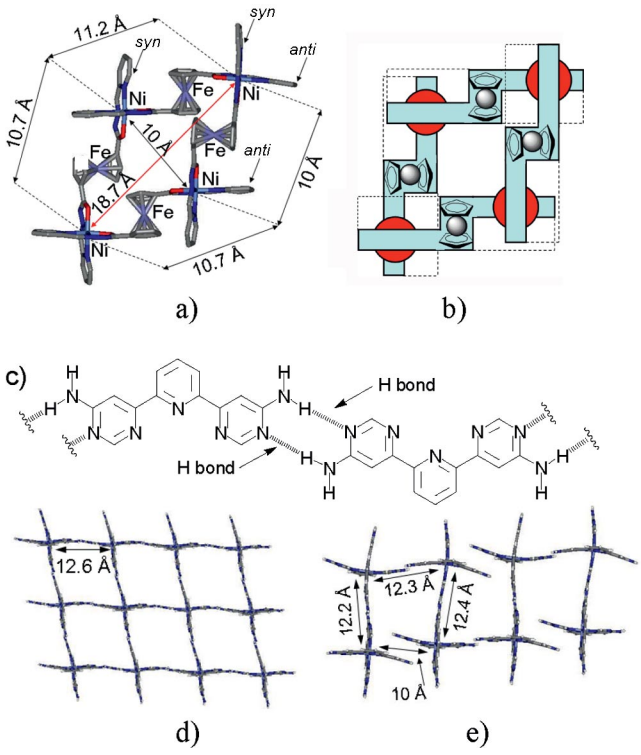

Figure 5. X-ray molecular structure (a; protons not shown; *anti* (*syn*) correspond to ligands where the two sites are *anti* (*syn*) oriented) and stylized representation (b) of grid $[Ni_4(\mathbf{3})_4]$;[11] (c) self-complementarity between ligands **1**; (d) grid-like polymeric network[12] generated by $[Co^{II}(\mathbf{1})_2](PF_6)_2$; (e) grid-like polymeric network[12] generated by $[Co^{III}_{0.5}Co^{II}_{0.5}(\mathbf{1})_2](BF_4)_{2.5}$ (anions, protons and solvent molecules omitted for clarity). Co–Co distances are given in (d) and (e).

3.1.2. Polymeric Grids

The "grids of nodes" generated by a one-site ligand and the polymeric "grids of grids" belong to this category.

3.1.2.1. Polymeric "Grids of Nodes"

Such grids may form from a monotopic ligand that has self-complementary ends. In such polymeric grids, in the solid state, the ligand can be seen as an extended polymeric ligand. A solid-state polymeric grid is generated by the monotopic ligand **1** (on reaction of its diamido-protected form with Co^{II} acetate in CH_3OH, followed by anion exchange with NH_4PF_6 or NH_4BF_4). The nodes $[Co(\mathbf{1})_2]^{x+}$ are connected by hydrogen bonds established between the self-complementary terminal 6-substituted-4-amino-pyrimidines (Figure 5c).[12] With PF_6^- as a counterion, the expected polymeric extended $[p \times p]$ grid is obtained (Figure 5d), and Co^{II} is predominantly high-spin. With BF_4^-, an extended grid is also obtained, but in one of the sides of the dissymmetric $[2 \times 2]$ grids that form the polymeric assembly, the hydrogen bond is not present (Figure 5e). In this last complex, Co centres are constituted from Co^{II} and Co^{III} in equal proportions, the average oxidation state being 2.5.

3.1.2.2. Polymeric "Grids of Grids"

They are examples of external high nuclearity. Extended $[2p \times 2p]$ bidimensional polymeric "grids of grids" formed of self-complementary $[Co_4(\mathbf{2a})_4]^{8+}$ grids generated by ligand **2a** were attempted, but a $[2 \times 2p]$ extended grid has been obtained (Figure 6).[13]

The Fe^{II}_4 $[2 \times 2]$ grid $[Fe_4(\mathbf{2b})_4]^{8+}$, in which four 4-substituted pyridine groups are located on the superior face and four on the inferior face (i.e. 8 Nsp^2 donor atoms, such grids being "complexes as ligands"), interacts with Ag^I cations to generate a solid-state polymeric self-assembled architecture $\{[Fe_4(\mathbf{2b})_4]Ag_4\}^{12+}$ (Figure 7).[14] Crystals are obtained at the interface between a solution of $[Fe_4(\mathbf{2b})_4](BF_4)_8$ in MeCN and a solution of 6 equiv. of $AgBF_4$ in MeOH. Similarly, the columnar coordination polymer $\{[Fe_4(\mathbf{2c})_4]La\}^{11+}$ was obtained from $[Fe_4(\mathbf{2c})_4](ClO_4)_8$ and an excess of 6 equiv. of $La(ClO_4)_3$.[14]

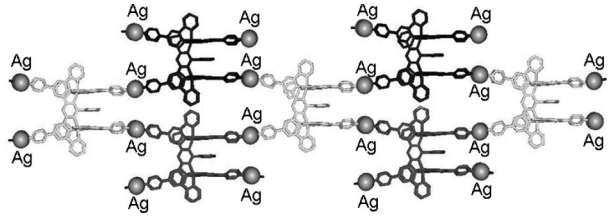

Figure 7. Lateral view of the self-assembled solid-state polymeric structure[14] $\{[Fe_4(\mathbf{2b})_4]Ag_4\}^{12+}$ obtained from grid $[Fe_4(\mathbf{2b})_4]^{8+}$ in the presence of Ag^I ions (anions, solvent molecules and protons not shown).

3.1.3. Complete $[s \times s]$ Grids ($5 \geq s \geq 3$)

In this case, the increase in the nuclearity is the direct consequence of the increase in the topicity of the ligand: tritopic ligands give $[3 \times 3]$ grids, tetratopic ones give $[4 \times 4]$ grids, *s*-site ligands would give $[s \times s]$ grids.

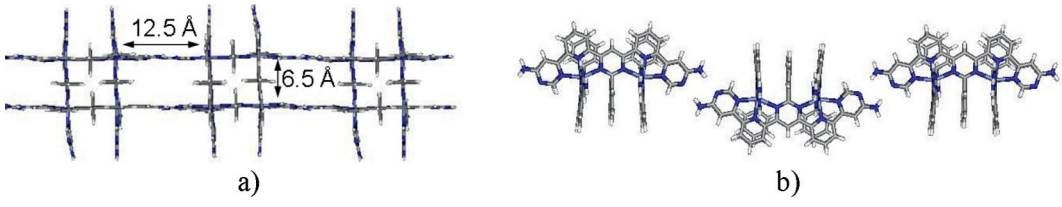

Figure 6. (a) Top view of the $[2 \times 2p]$ polymeric grid $\{[Co_4(\mathbf{2a})_4]^{8+}\}_p$ (Co–Co distances are indicated)[13]; (b) lateral view of the same polymeric grid.

3.1.3.1. Nonanuclear[15] [3 × 3] Grids

3.1.3.1.1. Grids Generated by a Ligand with Three Bidentate Sites A_1-A_2-A_3-A_4 ($A_1 = A_4 = py_1$ = 2-Substituted Pyridine, $A_2 = A_3 = pdz$ = 3,6-Disubstituted Pyridazine)

In the nonanuclear [3 × 3] grid-like complex $[Ag_9(\mathbf{7a})_6](CF_3SO_3)_9$ (ref.[16a]; Figure 8), Ag^I ions have a distorted tetrahedral coordination geometry. L_Cj and L_Ri ligands are expected to be perpendicular, and, consequently, angles Ag–Ag–Ag should be around 90°, but a difference of about 18° with respect to the theoretical angle is observed. In the parallelogram formed by the grid, the average distance between the C5 atoms of the terminal pyridine rings of a ligand is about 14.7 Å. The Ag–Ag diagonal distances are of about 12 and 8.8 Å.

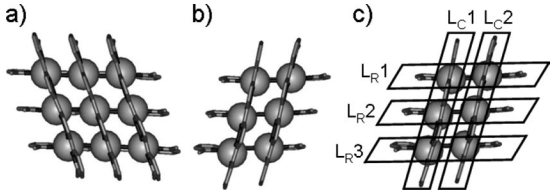

Figure 8. X-ray molecular structures of: (a) grid $[Ag_9(\mathbf{7a})_6]^{9+}$ (ref.[16a]); (b) grid $[Ag_6(\mathbf{4})_3(\mathbf{7a})_2]^{6+}$ (ref.[37a]) and its matrix-like representation (c) (protons, anions and solvent molecules omitted for clarity).

The self-assembly of grids $[Ag_9(\mathbf{7a,b})_6]^{9+}$ was found to occur in situ at the air–water interface,[16b] from the free ligands **7a**,**b** spread onto aqueous solutions containing Ag^+ ions, thus producing oriented crystalline films of grids.

3.1.3.1.2. Grids Generated by Ligands with Three Tridentate Sites A_1-B_1-A_2-B_2-A_3-B_3-A_4

3.1.3.1.2.1. Py_1-$(py_2$-pym$)_2$-py_2-py_1 Ligands (py_2 = 2,6-Disubstituted Pyridine, pym = 4,6-Disubstituted Pyrimidine)

The nonanuclear grid $[Pb_9(\mathbf{8a})_6](CF_3SO_3)_{18}$ (ref.[17]) formed by ligand **8a**, as well as grid $[Zn_9(\mathbf{8b})_6](BF_4)_{18}$,[18] were characterized by NMR spectroscopy (vide infra) and ES (electrospray) mass spectrometry. Grids $[Pb_9(\mathbf{8b})_6](CF_3SO_3)_{18}$ and $[Hg_9(\mathbf{8a})_6](CF_3SO_3)_{18}$ were characterized by ES mass spectrometry.[19]

3.1.3.1.2.2. Bis(acylhydrazone)s py_1-hyz-CO-py_2-CO-hyz-py_1 As Ligands

Particular interest is manifested for [3 × 3] grids generated by dideprotonatable tritopic ligands $\mathbf{9}H_2$ that belong to the class of bis(acylhydrazone)s.[20a] Usually, in such grids, the octahedral coordination environment of metal ions is *cis*-N_2O_4 for the corners (M_{11}, M_{13}, M_{31}, M_{33}), *mer*-N_3O_3 for the sides (M_{12}, M_{21}, M_{23}, M_{32}) and *trans*-N_2O_4 for the centre (M_{22}). Their average dimensions range from about 19 Å to about 22 Å.

3.1.3.1.2.2.1. Homometallic Grids

####### 3.1.3.1.2.2.1.1. Homometallic Copper(II) Grids

Ligand $\mathbf{9a}H_2$ reacts with $Cu(NO_3)_2{\cdot}3H_2O$ to produce grid $[Cu_9(\mathbf{9a}H)_6](NO_3)_{12}{\cdot}9H_2O$[21] (Figure 9a) and with $CuSO_4{\cdot}5H_2O$ to produce $[Cu_9(\mathbf{9a}H)_6](SO_4)_6{\cdot}18H_2O$.[21] The average Cu–Cu distance between adjacent Cu atoms is

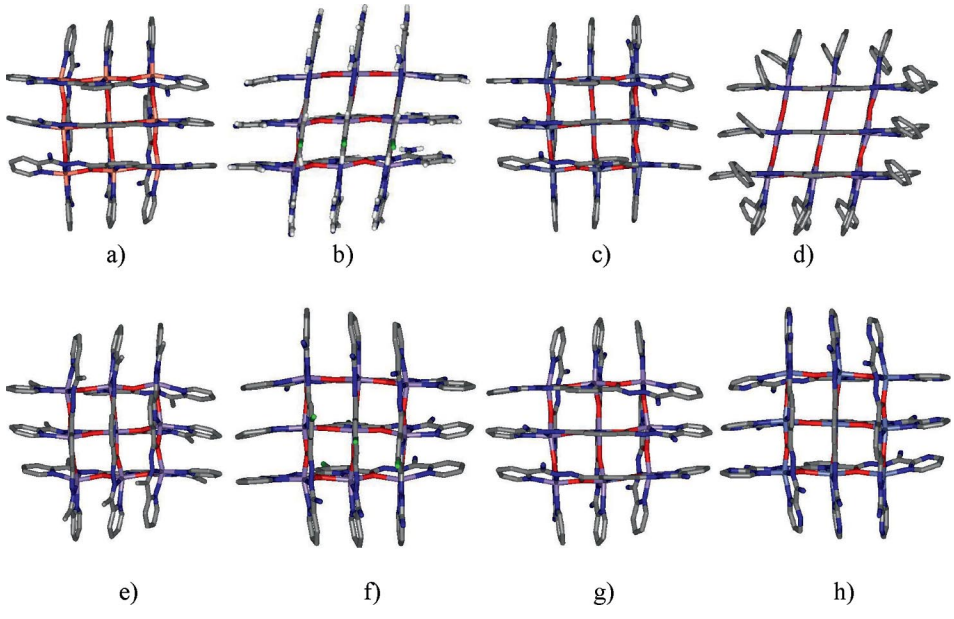

Figure 9. X-ray molecular structures of [3 × 3] grid-like complexes generated by tritopic bis(acylhydrazone) ligands (protons shown only for b; anions, solvent and water molecules omitted for clarity): (a) $[Cu_9(\mathbf{9a}H)_6](NO_3)_{12}{\cdot}9H_2O$;[21] (b) $[Mn_9(\mathbf{9j})_6](NO_3)_6{\cdot}22H_2O$;[26] (c) $[Zn_9(\mathbf{9a})_3(\mathbf{9a}H)_3](NO_3)_9{\cdot}24H_2O$;[24] (d) $[Mn_9(\mathbf{9g})_6](NO_3)_6{\cdot}12H_2O$;[24] (e) $[Mn_9(\mathbf{9f})_6](MnCl_4)_2Cl_2{\cdot}2CH_3OH{\cdot}7H_2O$;[24] (f) $[Mn_9(\mathbf{9b})_6](ClO_4)_9{\cdot}14H_2O{\cdot}3CH_3CN$;[27] (g) $[Mn_9(\mathbf{9a})_6](ClO_4)_{10}{\cdot}10H_2O$;[27] (h) $[Co_9(\mathbf{9k})_6](NO_3)_6{\cdot}24H_2O$.[29]

4.12 Å, and the average distance between the protons located on C5 of terminal py_1 groups of the same ligand is 19.7 Å.

Grid $[Cu_9(\mathbf{9k})_2(\mathbf{9k}H)_4](ClO_4)_{10}\cdot 13.2H_2O$[22] has Cu–Cu distances from 4.05 to 4.27 Å. It has fourfold symmetry. The central Cu_{22} has an axially compressed *trans*-N_2O_4 geometry with four long Cu–O distances and two short Cu–N ones. Side Cu^{II} ions (Cu_{12}, Cu_{23}, Cu_{21}, Cu_{32}) have a *mer*-N_3O_3 geometry with long axial Cu–O distances. Their Jahn–Teller axis passes through the two O atoms in *trans* and is perpendicular to the Jahn–Teller elongation axis of one corner Cu^{II} ion (Figure 10); thus, each corner Cu^{II} has an orthogonal magnetic connection with one of its neighbouring side Cu^{II} ions.[22]. Grids $[Cu_9(\mathbf{9b}H)_3(\mathbf{9b})_3](NO_3)_9\cdot 20H_2O$ and $[Cu_9(\mathbf{9d}H)_2(\mathbf{9d})_4](NO_3)_8\cdot 17H_2O$ were also reported.[23]

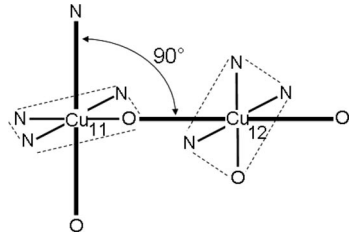

Figure 10. Perpendicular N–Cu_{11}–N and O–Cu_{12}–O Jahn–Teller axes causing orthogonal magnetic interactions in the fourfold symmetrical grid $[Cu_9(\mathbf{9k})_2(\mathbf{9k}H)_4](ClO_4)_{10}\cdot 13.2H_2O$[22].

3.1.3.1.2.2.1.2. Homometallic Manganese Grids

3.1.3.1.2.2.1.2.1. Homometallic Homovalent Manganese(II) Grids

The [3 × 3] Mn_9 grids $[Mn_9(\mathbf{9a})_6](N(CN)_2)_6\cdot 10H_2O$ (Mn–Mn diagonals of 10.78 and 10.78 Å), $[Mn_9(\mathbf{9a})_6]_2[Mn(NCS)_4(H_2O)]_2(NCS)_8\cdot 10H_2O$ (Mn–Mn diagonals of 11.50 and 10.72 Å), $[Mn_9(\mathbf{9i})_6](NO_3)_6\cdot 14.5H_2O$ (Mn–Mn diagonals of 10.78 and 10.66 Å), $[Mn_9(\mathbf{9g})_6](NO_3)_6\cdot 12H_2O$ (Figure 9d; Mn–Mn diagonals of 9.8 and 12.11 Å), $[Mn_9(\mathbf{9f})_6](MnCl_4)_2Cl_2\cdot 2CH_3OH\cdot 7H_2O$ (Figure 9e; Mn–Mn diagonals of 10.53 and 10.53 Å) and $[Mn_9\{(\mathbf{9c}H_2)_6\text{-}8H\}](ClO_4)_{10}\cdot 12H_2O$ were reported.[24] Mn–Mn distances are from 3.87 to 4.03 Å.

The X-ray crystal structures of grids $[Mn_9(\mathbf{9a})_6](ClO_4)_6\cdot 3.57MeCN\cdot 11H_2O$,[25] $[Mn_9(\mathbf{9j})_6](NO_3)_6\cdot 22H_2O$ (Figure 9b; average Mn–Mn distances of about 3.91 Å), $[Mn_9(\mathbf{9b})_6](ClO_4)_6\cdot 10H_2O$ (average Mn–Mn distances of about 3.98 Å),[26] $[Mn_9(\mathbf{9k})_6](NO_3)_6\cdot 28H_2O$[22] (average Mn–Mn distances of about 3.92 Å) and $[Mn_9(\mathbf{9a})_6](NO_3)_6\cdot 14H_2O$[27] present structural features common to this grid family.

The grids $[Mn_9(\mathbf{9d})_6](ClO_4)_6\cdot 22H_2O$,[27] $[Mn_9(\mathbf{9f})_6](PF_6)_6\cdot 3H_2O\cdot 4CH_3OH\cdot 2CH_3CN$,[47] $[Mn_9(\mathbf{9l})_6](ClO_4)_6\cdot 16H_2O$,[47] $[Mn_9(\mathbf{9c})_6](CF_3SO_3)_6\cdot 26H_2O$,[47] $[Mn_9(\mathbf{9c})_6](NCS)_6\cdot 13H_2O\cdot 3CH_3OH$,[47] $[Mn_9\{(\mathbf{9c}H_2)_6\text{-}8H\}](ClO_4)_{10}\cdot 12H_2O$[24] were reported as well.

Within grid $[Mn_9(\mathbf{9e})_6](ClO_4)_6\cdot 8H_2O$,[28] ligands L_Cj coordinate by means of two terminal N_2O sites and one central NO_2 site (Figure 11), while ligands L_Ri coordinate by means of two terminal N_2O sites and one central N_3 site, a fact that gives this grid an "alternate" aspect and may be due to some steric hindrance caused by quinoline units in a "normal" grid, but not in the "alternate" one. Its average dimensions are 21.7 Å × 20.3 Å.

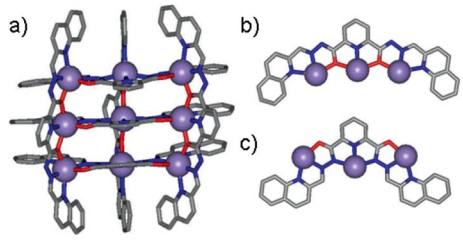

Figure 11. (a) X-ray structure of grid $[Mn_9(\mathbf{9e})_6]^{6+}$ (ref.[28]); (b) N_2O–NO_2–N_2O and (c) N_2O–N_3–N_2O coordination modes of ligand $\mathbf{9e}^{2-}$ in the corresponding grid (protons not shown; vide infra Figure 12c,d).

3.1.3.1.2.2.1.2.2. Homometallic Heterovalent Manganese Grids

Grids $[Mn^{III}_3Mn^{II}_6(\mathbf{9b})_6](ClO_4)_9\cdot 7H_2O$ (Mn–Mn diagonals of 11.24 and 11.08 Å; Mn^{III} located at three corners), $[Mn^{III}_3Mn^{II}_6(\mathbf{9b})_6](ClO_4)_9\cdot 10H_2O$ (both grids were obtained by chemical oxidation of $[Mn_9(\mathbf{9b})_6](ClO_4)_6\cdot 10H_2O$ with Cl_2), $[Mn^{III}_3Mn^{II}_6(\mathbf{9b})_6](ClO_4)_9\cdot 6H_2O$ (obtained by electrochemical oxidation of $[Mn_9(\mathbf{9b})_6](ClO_4)_6\cdot 10H_2O$) were reported.[24] In grid $[Mn^{III}_3Mn^{II}_6(\mathbf{9b})_6](ClO_4)_9\cdot 14H_2O\cdot 3CH_3CN$ (Figure 9f), synthesized by oxidation of $[Mn_9(\mathbf{9b})_6](ClO_4)_6\cdot 10H_2O$ with Br_2, the three Mn^{III} are also located at three corners.[27]

In the $Mn^{III}_4Mn^{II}_5$ heterovalent grid $[Mn_9(\mathbf{9a})_6](ClO_4)_{10}\cdot 10H_2O$ (Figure 9g) obtained by electrochemical oxidation of $[Mn_9(\mathbf{9a})_6](ClO_4)_6\cdot 18H_2O$, Mn^{III} ions are also located at the corners.[27]

3.1.3.1.2.2.1.3. Homometallic Grids with Other Metals (Co, Ni, Zn, Fe)

Grid $[Co^{II}_9(\mathbf{9k})_6](NO_3)_6\cdot 24H_2O$[29] (Figure 9h) belongs to the family of "complexes as ligands" that have free, potentially coordinating groups or donor atoms, like NH_2 or pyrimidine Nsp^2. The distance between the H atoms located on C4 of the terminal pyrimidine groups is about 19.4 Å, and Co–Co diagonals are about 10.9 Å.

Grid $[Zn_9(\mathbf{9a})_3(\mathbf{9a}H)_3](NO_3)_9\cdot 24H_2O$[26] (Figure 9c) has the average square side of 19.7 Å, Zn–Zn diagonals of about 11 Å and distances between adjacent Zn cations from 3.91 to 4.12 Å.

Grids $[Ni^{II}_9(\mathbf{9i})_4](BF_4)_6\cdot 12H_2O$,[30] $[Co^{II}_9(\mathbf{9a}H)_3(\mathbf{9a})_3](NO_3)_9\cdot 9H_2O$[30] and $[Fe^{III}_9(\mathbf{9a})_6](NO_3)_{15}\cdot 18H_2O$[26] were also reported.

3.1.3.1.2.2.1.4. "Normal" versus "Alternate" Complete Grids

The coordination mode of the central unit A_2-B_2-A_3 of row ligands L_Ri determines the nature of the grid: (i) "normal" [3 × 3] grid (Figure 12a,c), where the "NO_2 mode" is

adopted (A_2 = **CO**, B_2 = py_2, A_3 = **CO**), or (ii) "alternate" [3 × 3] grid (Figure 12b,d) where the "N_3 mode" is adopted (A'_2 = **OCN**–, B_2 = py_2, A'_3 = **OCN**–). In "normal" grids, the coordination mode for both L_Cj and L_Ri ligands (i, j = 1–3) is N_2O–NO_2–N_2O (Figure 12a,c), while in "alternate" grids, L_Cj ligands act as N_2O–NO_2–N_2O (Figure 11b, Figure 12c), but L_Ri ligands act as N_2O–N_3–N_2O (Figure 11c, Figure 12d).

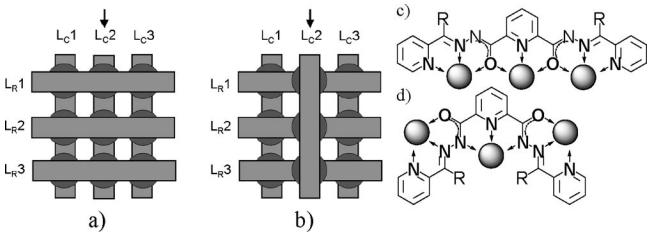

Figure 12. Representation of: (a) a "normal" [3 × 3] grid; (b) an "alternate" [3 × 3] grid; (c) N_2O–NO_2–N_2O coordination mode; (d) N_2O–N_3–N_2O coordination mode.

3.1.3.1.2.2.2. Heterometallic Grids

Such grids are fascinating and intriguing. Theoretically, a formula that corresponds to a heteronuclear grid $[(M_1)_r(M_2)_{9-r}L_6]^{x+}$, may also correspond to a mixture of homonuclear grids $r/9[(M_1)_9L_6]^{x+}$ + $(1 - r/9)[(M_2)_9L_6]^{x+}$. One may wonder why the heterometallic grid forms instead of the mixture of homometallic grids mentioned and why the metal ions are located in the current positions. Structural (ionic radii) and energetic factors could explain their formation. For the moment, there are no studies performed in solution, which might provide information on whether their formation is quantitative and what the equilibria involved would be.

Grid $[Mn^{II}_5Zn^{II}_4(\mathbf{9k})_6](NO_3)_6{\cdot}33H_2O{\cdot}20CH_3OH$[29] (Figure 13a) was obtained by the reaction of $\mathbf{9k}H_2$ with 1.5 equiv. of $Mn(NO_3)_2{\cdot}6H_2O$, followed by addition of 0.9 equiv. of $Zn(CH_3COO)_2{\cdot}2H_2O$, heating and a period of crystal growth. The four Zn^{II} ions occupy the side positions (12, 23, 32, 21), while Mn^{II} cations are located at the corners and at the centre. Zn–Zn diagonals are 10.84 Å, and grid average dimensions are 19.4 Å × 19.4 Å.

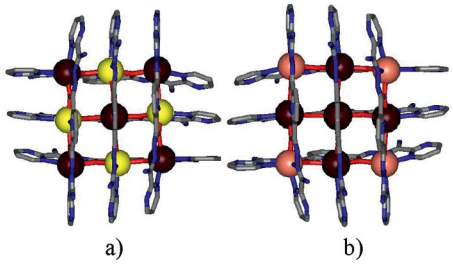

Figure 13. X-ray molecular structure (protons, anions, solvent, water molecules not shown) of grids:[29] (a) $[Mn^{II}_5Zn^{II}_4(\mathbf{9k})_6]^{6+}$; Mn^{II} ions are located at the centre and corners, and Zn^{II} ions are located at side positions; (b) $[Mn^{II}_5Cu^{II}_4(\mathbf{9k})_6]^{6+}$; Cu^{II} ions are located at the corners, and Mn^{II} ions are located at central and side positions.

A kind of substitution reaction on $[Mn^{II}_9(\mathbf{9k})_6](NO_3)_6{\cdot}28H_2O$ yielded two other heterometallic grids. After its treatment with NaOH to reach a neutral pH, addition of 5 equiv. of $Cu(NO_3)_2{\cdot}6H_2O$ followed by addition of Et_3N to keep the pH neutral, crystals of grid $[Mn^{II}_5Cu^{II}_4(\mathbf{9k})_6](NO_3)_6{\cdot}15H_2O{\cdot}2CH_3OH$[29] (Figure 13b) were obtained after several days. Such reactions appear to be very interesting, because such substitution process should involve disassembly of at least a part of the grid. Cu^{II} cations are located at the corners, and the *trans* oriented N–Cu bonds given by the N atoms are compressed. Average grid dimensions are 19.4 Å × 19.4 Å, and Mn–Mn diagonals are 11 Å.

Reaction of $[Mn^{II}_9(\mathbf{9k})_6](NO_3)_6{\cdot}28H_2O$ with 24 equiv. of $Cu(NO_3)_2{\cdot}6H_2O$ at reflux yielded grid $[Mn^{II}Cu^{II}_8(\mathbf{9k})_6](NO_3)_6{\cdot}23H_2O$[29]. The Mn^{II} ion occupies the central position of the grid. Cu^{II} ions present a Jahn–Teller deformation that generate orthogonal magnetic connections between Cu^{II} ions, but the Mn–Cu connections are not orthogonal (ferrimagnetic interaction allowed).

The grid $[Mn^{II}_8Co^{II}(\mathbf{9i})_6](ClO_4)_6{\cdot}14H_2O{\cdot}3CH_3OH$[47] was reported as well.

3.1.3.2. Hexadecanuclear [4 × 4] Grids

3.1.3.2.1. Hexadecanuclear [4 × 4] Lead(II) Grids

The Pb_{16} [4 × 4] grid generated by ligand **11** upon reaction with two equivalents of $Pb(CF_3SO_3)_2$ was firstly characterized by NMR spectroscopy.[17] Its X-ray structure[31] (Figure 14a) showed that the solid-state complex cation is $[Pb_{16}(\mathbf{11})_8(CF_3SO_3)_{16}(H_2O)_8]^{16+}$, which can be described as a set of four [2 × 2] sub-grids. The average Pb–Pb distance is 6.3 Å. Pb^{II} are hepta-, octa-, or nonacoordinated. Pb–Pb diagonals are 26.9 and 26.3 Å. The average distance between C4 atoms of a ligand in the grid is 28.8 Å.

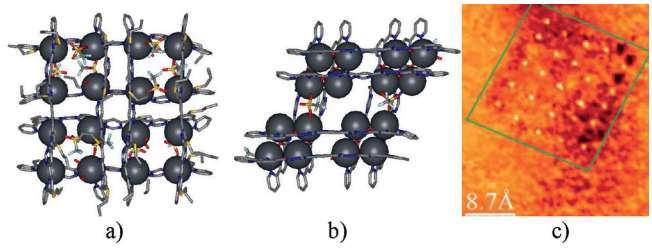

Figure 14. (a, b) X-ray molecular structures of the hexadecanuclear Pb^{II} grids generated by ligands (a) **11** (ref.[31]) and (b) $\mathbf{13}^{2-}$ (ref.[32]) (protons, water molecules and several anions omitted for clarity); (c) STM/CITS measurements for the Mn_{25} [5 × 5] complex showing the CITS current image recorded at –0.732 V; reprinted with permission from ref.[28]; copyright 2007 American Chemical Society.

The [2 × 2] sub-grids, contained in polymeric (vide supra) or discrete high-nuclearity complete grids in which the metal ions are separated by pyrimidine rings (M,N,C,N,M sequences), belong to the class of expanded azametallacrowns [16-MC_M-4] (MC is the abbreviation for metallacrown,[3c] and the subscript M is Co, Fe, Zn, Pb or Hg).

Reaction of ligand $\mathbf{13}H_2$ with 2 equiv. of $Pb(CF_3SO_3)_2$ yielded the [4 × 4] grid $[Pb_{16}(\mathbf{13})_8(CF_3SO_3)_6(H_2O)_5](CF_3SO_3)_{10}{\cdot}23H_2O$.[32] It appears as a puckered square (Fig-

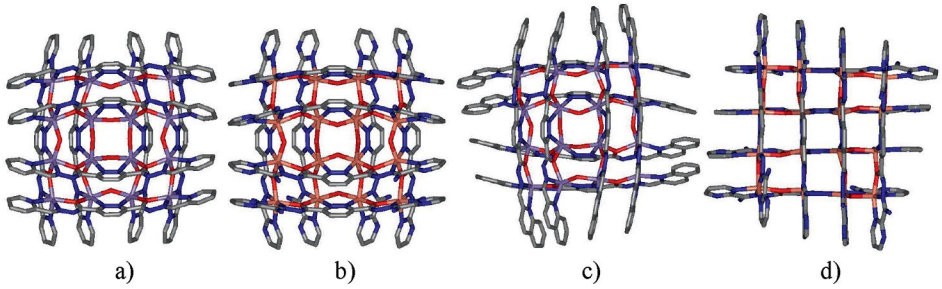

Figure 15. X-ray structures of grids (protons not shown): (a) $[Mn_{16}(\mathbf{10b})_8(OH)_8]^{8+}$ (ref.[28]); (b) $[Cu_{16}\{(\mathbf{10d})_8\text{-}2H\}(O)_2(OH)_4(H_2O)_2]^{6+}$ (ref.[34]); (c) $[Mn_{16}(\mathbf{10c})_8(O)_4(OH)_4]^{4+}$ (ref.[29]); (d) $[Cu^{II}_{12}Cu^{I}_{4}(\mathbf{10d})_8]^{12+}$ (ref.[29]).

ure 14b), the average distance between the protons on C4 atoms of terminal pyridines of the same ligand being 27.4 Å and Pb–Pb diagonals 15.9 and 27.5 Å. It can be described as a $[4\times(2\times2)]$ grid; the bridging group between the two Pb^{II} in the $[2\times2]$ grid is a $C\text{–}O^-$ (Pb–Pb distances 7.0–7.8 Å), and the one connecting the $[2\times2]$ grids is a pyrimidine ring (Pb–Pb distances 4.1–4.4 Å).

Both of the grids discussed above are of general formula $[Pb_{16}L_8(L')_\alpha(L'')_\beta]^{x+}$ where $L' = CF_3SO_3^-$ and $L'' = H_2O$. The 16 metal ions and 8 tetratopic ligands corresponding to a complete $[4\times4]$ grid are present, but there are also two other types of ligands: triflate and water.

Reaction of ligand **12** with two equivalents of $Pb(CF_3SO_3)_2$ in nitromethane produces the $[4\times4]$ grid-like complex $[Pb_{16}(\mathbf{12})_8](CF_3SO_3)_{32}$, which was characterized by 1D and 2D NMR spectroscopy (vide infra).[33]

3.1.3.2.2. Hexadecanuclear [4×4] Manganese(II) Grids

In grid $[Mn_{16}(\mathbf{10b})_8(OH)_8](NO_3)_8\cdot15H_2O$[28] (Figure 15a), eight HO^- ligands act as bridging ligands between Mn_{12} and Mn_{13}, Mn_{21} and Mn_{31}, Mn_{22} and Mn_{23}, Mn_{24} and Mn_{34}, Mn_{32} and Mn_{33}, Mn_{42} and Mn_{43} (the subscript indicates the position in the matrix-like representation of this grid, not shown, but easily imaginable; for an example of numbering of metal ions, see Figure 28a). The average dimensions (distances between the protons located on C5 atoms of terminal pyridines of a coordinated ligand) of the grid are 20.5 Å × 20.5 Å. Grid $[Mn_{16}(\mathbf{10b})_8(OH)_8](ClO_4)_8\cdot15H_2O$, with a similar structure, was also reported.[28]

Ligand **10c** generated the hexadecanuclear grid $[Mn_{16}(\mathbf{10c})_8(O)_4(OH)_4](NO_3)_4\cdot42H_2O\cdot4CH_3CN$[29] (Figure 15c) with Mn–Mn distances from 3.9 to 4.1 Å and average dimensions of 24.4 Å × 24.4 Å. Four O^{2-} bridging ligands connect two-by-two neighbouring metal ions from the sides of the grid (i.e. Mn_{12} and Mn_{13}, Mn_{21} and Mn_{31}, Mn_{42} and Mn_{43}, Mn_{24} and Mn_{34}), and four HO^- ligands connect two-by-two the central neighbouring metal ions (Mn_{22} and Mn_{23}, Mn_{23} and Mn_{33}, Mn_{33} and Mn_{32}).

3.1.3.2.3. Hexadecanuclear [4×4] Copper Grids

In grid $[Cu^{II}_{16}\{(\mathbf{10d})_8\text{-}2H\}(O)_2(OH)_4(H_2O)_2](CF_3SO_3)_6\cdot66H_2O\cdot10CH_3OH$[34] (Figure 15b), composed of four identical $[2\times2]$ sub-grids, the average Cu–Cu distance is 4 Å, the Cu–Cu diagonal is 15.5 Å, and the average distance between the protons on C5 atoms of terminal pyrimidines is 20.8 Å. Small ligands like H_2O, HO^-, O^{2-} are required to complete the coordination environment of Cu^{II} centres, and it is likely that an incomplete grid, as for example the "frame" containing 12 Cu^{II} ions,[38] would have formed without them. These bridging ligands act in the following mode: H_2O connects Cu_{12} and Cu_{13}, Cu_{42} and Cu_{43}, HO^- connects Cu_{21} and Cu_{31}, Cu_{22} and Cu_{32}, Cu_{23} and Cu_{33}, Cu_{24} and Cu_{34}, and O^{2-} connects Cu_{22} and Cu_{23}, and Cu_{32} and Cu_{33}. In the *mer*-N_3O_3 coordination sphere of side Cu^{II} ions, only five donor atoms belong to ligands $\mathbf{10d}^{2-}$, the sixth belonging to a water molecule or a HO^- group (vide supra the general representation in Figure 1d). In the *trans*-N_2O_4 coordination sphere of central Cu_{22}, Cu_{23}, Cu_{32} and Cu_{33}, one O atom belongs to a HO^- group, another one to an oxide O^{2-}, and the others belong to ligands $\mathbf{10d}^{2-}$.

To obtain the heterovalent grid-like complex $[Cu^{II}_{12}Cu^{I}_{4}(\mathbf{10d})_8](CF_3SO_3)_{12}\cdot24H_2O$[29] (Figure 15d), the 1:2 ligand/$Cu(CF_3SO_3)_2$ mixture was treated with $K[Ag(CN)_2]$. On the basis of bond valence sum (BVS) calculations, ions corresponding to 22, 23, 33 and 32 elements in the matrix-like representation (not shown) were designed as Cu^I. They have a N_2O_2 coordination sphere. The distance between two adjacent Cu^I atoms is 3.32 Å, the average distance between other kinds of adjacent copper ions being 3.95 Å. Corner-located Cu^{II} atoms have a *cis*-N_4O_2 coordination sphere, while side-located ones have a N_3O_2 sphere. The average dimensions of the grid are 20.8 Å × 20.8 Å.

3.1.3.3. Pentacosanuclear [5×5] Grids[28]

Grid $[Mn_{25}(\mathbf{15H})_{10}](ClO_4)_{20}\cdot65H_2O$ generated by the pentatopic ligand $\mathbf{15H}_4$ upon reaction with $Mn(ClO_4)_2\cdot6H_2O$ was investigated by STS/CITS imagery on highly ordered pyrolytic graphite (HOPG) (Figure 14c), and the positions of the Mn atoms describe a $[5\times5]$ array whose edge is 17 Å, in accordance with the sum of four Mn–Mn distances of about 4 Å each (as deduced from the previous structures of Mn grids with ligands from the same family). Treatment of this grid with Et_3N gave a compound that should be the grid of the fully deprotonated ligand $[Mn_{25}(\mathbf{15})_{10}]^{10+}$.

3.1.4. Heteroleptic Complete [m×n] Grids (m ≠ n)

This type of grid contains two kinds of polytopic ligands, *m n*-site ligands and *n m*-site ligands, as well as $m\times n$ metal ions, being of general formula $[M_{m\times n}(L^m)_n(L^n)_m]^{x+}$, where

L^m is an *m*-site ligand and L^n is an *n*-site one. Only [2 × 3] grids (*m* = 2, *n* = 3) of this kind were reported until now.

In the silver(I) grid of this kind reported,[37a] M is Ag^I, L^3 is **7a** and L^2 is **4** (i.e. 6,6′-bis(6-methyl-2-pyridyl)pyridazine) (Figure 2c). The mixture **3/7a**/$AgCF_3SO_3$ (3:2:6) in CD_3NO_2 contains 90% of grid $[Ag_6(\mathbf{4})_3(\mathbf{7a})_2](CF_3SO_3)_6$. The X-ray molecular structure (Figure 8c) of the grid is like a rhombus whose small angles are 66°, Ag–Ag diagonals are 6.9 Å (Ag_{11}–Ag_{32}) and 9.7 Å (Ag_{12}–Ag_{31}), and sides (i.e. distances between the protons located on C5 atoms of the terminal py_1 of a ligand) are 13 and 17 Å.

Di- (**5**) and tritopic (**6**) ligands incorporating two and three phenanthroline-derived bidentate sites connected through 1,4-diethynyl-benzene units, respectively, were synthesized in the framework of the interesting HETPHEN concept,[37b] where bulky aryl substituents (like R^1 and R^3 in **5a** and **6a**; see Figure 2c) produce steric and electronic effects inducing the shift of the coordination equilibrium toward the formation of heteroleptic complexes. [2 × 3] heteroleptic hexanuclear grids[37c] $[Cu_6(\mathbf{5a})_3(\mathbf{6b})_2]^{6+}$ (Figure 16) and $[Cu_6(\mathbf{5b})_3(\mathbf{6a})_2]^{6+}$ slowly form as the product of the reaction of **5a** and **6b** and **5b** and **6a**, respectively, with $[Cu(MeCN)_4]PF_6$ in dichloromethane (**5/6**/Cu^I = 3:2:6). The distance between the Cu^I ions located in two consecutive sites of a ligand of type **5** or **6** is 17 Å.[37c] According to models, the dimensions of grid $[Cu_6(\mathbf{5a})_3(\mathbf{6b})_2]^{6+}$ are 29 and 60 Å (corresponding to a rectangular surface of 1740 Å^2); its diagonal is 50 Å.

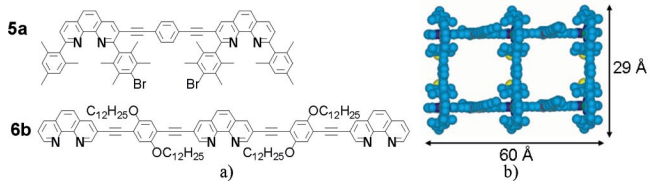

Figure 16. (a) Structural formulas of ligands **5a** and **6b**; (b) Hyperchem representation of the [2 × 3] grid $[Cu_6(\mathbf{5a})_3(\mathbf{6b})_2]^{6+}$ from ref.[37c]; reproduced by permission of the Royal Society of Chemistry.

3. 1. 5. A Catenane

An octanuclear [2]catenane[37d] consisting of two [2 × 2] grids can be seen as a way to increase the nuclearity.

3.2. Incomplete Grids

An incomplete grid is a grid generated by an *s*-site ligand where one or more of 2*s* ligands and/or of s^2 metal ions are missing. Within the class of incomplete grids, there are:

– metal-defective grids (grids in which all expected 2*s* ligands are present, but several metal ions are missing, i.e. M_y [*s* × *s*] grid-like complexes, where $y < s^2$);

– ligand-defective grids (grids in which all expected cations are present, but one or several *s*-topic ligands are missing, i.e. M_{s^2} [*m* × *n*] grid-like complexes, where $m \leq s$ and $n < s$);

– metal-and-ligand defective grids (grids in which one or several *s*-site ligand(s) and several cations are missing, with respect to the expected complete [*s* × *s*] grid, i.e. M_y [*m* × *n*] grid-like complexes, where $y < s^2$, $m \leq s$ and $n < s$).

For a matrix-like representation of these three kinds of grids, see the Supporting Information.

3.2.1. Metal-Defective Grids

This class comprises grids generated by tritopic ligands and grids generated by tetratopic ligands.

3.2.1.1. Grids Generated by Tritopic Ligands

In grid $[Fe^{III}_5(\mathbf{9b}H)_6](ClO_4)_9 \cdot 34.5H_2O$[26] (Figure 17e,f), the side metal centres, that is, 12, 23, 32, 21, are missing. The average distance between the protons located on atom C4 of the terminal pyridines is 19.6 Å. Fe–Fe diagonals are 10.98 and 10.72 Å. The formation of this grid[26] might pass through a tetranuclear [2 × 2] intermediate containing only L_C1, L_C3, L_R1 and L_R3 as ligands and Fe_{11}, Fe_{13}, Fe_{31} and Fe_{33} as metal ions (thus positioned at the corners to avoid the central chloro-substituted pyridine rings that should be weaker donors). This [2 × 2] intermediate would further accommodate the unit containing ligands L_R2 and L_C2 and the metal ion Fe_{22}. This unit would form through the insertion of, for example, L_R2 – with Fe_{22} already bound to the

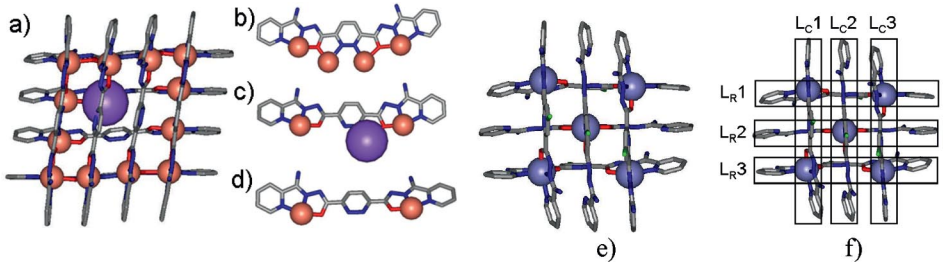

Figure 17. (a) X-ray molecular structure of grid $[Cu_{12}Na(\mathbf{10a})_8]^{9+}$ (ref.[38]); (b), (c), (d) coordination modes of ligand $\mathbf{10a}^{2-}$ in the complex cation $[Cu_{12}Na(\mathbf{10a})_8]^{9+}$ (protons not shown); X-ray molecular structure (e) and matrix-like representation (f) of grid $[Fe^{III}_5(\mathbf{9b}H)_6]^{9+}$ (ref.[26]; protons, anions and water molecules not shown).

central NO_2 site (-CO-py-CO-) – between L_R1 and L_R3, simultaneously with the insertion of L_C2 between L_C1 and L_C3 and the binding of Fe_{22} to the central free tridentate site of L_C2. This insertion, as well as the complete unbending (vide infra) of the ligand seems to be made easier by the attractive interaction between the terminal pyridines of L_C2 and L_R2 – pyridines that are uncoordinated and consequently more electron-rich – and between L_C1 and L_C2 and L_R1 and L_R2, respectively, pyridines that are bound to the corner Fe^{III} ions and consequently electron-poor.

3.2.1.2. Grids Generated by Tetratopic Ligands

Tridecanuclear grid $[Cu_{12}Na(\mathbf{10a})_8](BF_4)_9{\cdot}21H_2O{\cdot}2CH_3OH$[38] (Figure 17a) is obtained by reaction of ligand $\mathbf{10a}H_2$ with $Cu(CH_3COO)_2{\cdot}2H_2O$ in methanol (the molar ratio $\mathbf{10a}H_2/Cu^{II}$ was 1:1 or 3:4) followed by precipitation with $NaBF_4$. A grid-like motif $[Cu_{12}(\mathbf{10a})_8]^{8+}$ was obtained when NH_4BF_4 was used instead of $NaBF_4$. This fact suggest that Na^+ does not play any role in the self assembly of the $[Cu_{12}(\mathbf{10a})_8]^{8+}$ "frame", being encapsulated within this "frame" on addition of $NaBF_4$. The dideprotonated ligands $\mathbf{10a}^{2-}$ adopt three coordination modes, binding to four Cu^{II} cations (Figure 17b), or to two Cu^{II} and one Na^I cations (Figure 17c) or, alternatively, to two Cu^{II} cations (Figure 17d). Among the 12 Cu^{II} cations, the corner ones (Cu_{11}, Cu_{14}, Cu_{41}, Cu_{44}) have pseudo-O_h coordination geometry, while the others (Cu_{12}, Cu_{13}, Cu_{21}, Cu_{31}, Cu_{42}, Cu_{43}, Cu_{34}, Cu_{24}) have a square-pyramidal geometry. The sodium(I) cation has a distorted T_d coordination geometry; it is not statistically distributed over the four central N_2O_2 sites. Such N_2O_2 tetrahedral coordination environments seem not to be preferred by Cu^{II}, a fact that may explain why they are unoccupied.[38] Indeed, complete grids of ligand $\mathbf{10}^{2-}$ were obtained with four Cu^I ions located in these tetrahedral sites[29](vide supra), or with supplementary small ligands (like O^{2-} or HO^-) that complete these sites by transforming them into *mer*-N_3O_3 sites appropriate for Cu^{II} ions[29,34](vide supra). The conformation of the simple bonds that connect the uncoordinated pyridazine rings to neighbouring hydrazones is *transoid* (Figure 17d); it is *cisoid* in occupied sites. The average distance between the protons located on C5 atoms of terminal pyridine rings of the coordinated ligands is about 20.9 Å.

Grid $[Cu_{12}(\mathbf{10a})_8Na_{1.53}](NO_3)_{9.53}{\cdot}30H_2O$[35] was obtained by the reaction of $[Ni_3(\mathbf{10a}H)_3(H_2O)](NO_3)_3{\cdot}2H_2O$[36] with four equivalents of $Cu(NO_3)_2{\cdot}6H_2O$. The frame, constituted of 8 ligands and 12 Cu ions (as in grid $[Cu_{12}Na(\mathbf{10a})_8](BF_4)_9{\cdot}21H_2O{\cdot}2CH_3OH$, vide supra), is filled with sodium cations whose partial occupancy is 0.25, 0.125, 0.5 and 0.65. The average distance between the protons located on C4 atoms of the terminal pyridine ring is 20.9 Å.

3.2.2. Ligand-Defective Grids. Heteroleptic Complex Cations $[M_9L_5(L')_\alpha(L'')_\beta(L''')_\gamma]^{x+}$

In this case, one or more *s*-site polytopic ligand(s) is (are) replaced by several monotopic ligands that complete the coordination environment of the metal ions that should have been bound to missing ligand(s). There is a difference between this kind of incomplete grid and the complete heteroleptic [$m \times n$] grid in which all expected elements of the grid are present.

In grid $[Cu_9(\mathbf{9a}H)_4(COOC_5H_3NCOOH)_3(COOC_5H_3NCOO)(H_2O)](NO_3)_9{\cdot}8H_2O$[23] (Figure 18a), ligands L_R1 and L_R3 are missing and are replaced by one water molecule, one dideprotonated and three monodeprotonated molecules of pyridine-2,6-dicarboxilic acid. Cu_{21} (*mer*-N_3O_3), Cu_{22} (*trans*-N_2O_4) and Cu_{23} (*mer*-N_3O_3) are coordinated as in a complete grid. Cu_{11}, Cu_{13}, Cu_{31} and Cu_{33} have *mer*-N_3O_3 coordination spheres, Cu_{12} has a N_2O_3 sphere, and Cu_{32} has a *cis*-N_2O_4 sphere.

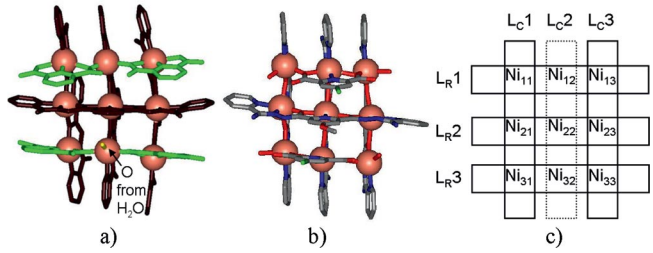

Figure 18. X-ray molecular structures (protons not shown) of grids $[Cu_9(\mathbf{9a}H)_4(COOC_5H_3NCOOH)_3(COOC_5H_3NCOO)]^{9+}$ (ref.[23]) (a) and $[Cu_9(\mathbf{9d})_4(COOC_5H_2ClNCOO)_2(H_2O)_4]^{6+}$ (ref.[39]) (b); (c) stylized matrix-like representation of grid $[Ni_9(\mathbf{9h})_5(OH)_2(CH_3CN)_2(H_2O)_3]^{6+}$ (ref.[40]) (only metal centres and ligands $\mathbf{9h}^{2-}$ are represented; the missing ligand L_C2 is shown as a rectangle with dashed lines).

Similarly, in grid $[Cu_9(\mathbf{9d})_4(COOC_5H_2ClNCOO)_2(H_2O)_4](NO_3)_6{\cdot}22H_2O$[39] (Figure 18b), ligands L_R1 and L_R3 are missing and are replaced by four water molecules and two dideprotonated molecules of 4-chloropyridine-2,6-dicarboxylic acid. Cu ions from row 2 have the expected coordination environment, as in the grid above. Cu_{11}, Cu_{13}, Cu_{31} and Cu_{33} have an N_2O_3 coordination environment that includes the O atom of a water molecule and an O atom of a carboxylate group. Cu_{12} and Cu_{32} have *mer*-N_3O_3 coordination spheres.

In grid $[Ni_9(\mathbf{9h})_5(OH)_2(CH_3CN)_2(H_2O)_3](ClO_4)_6{\cdot}19H_2O$[40] (for the matrix-like representation of the $[Ni_9(\mathbf{9h})_5]^{8+}$ part of the complex cation, see Figure 18c), the central ligand L_C2 is missing, and the coordination sphere of the three corresponding Ni^{II} cations is completed by HO^-, H_2O and CH_3CN, the central Ni_{22}^{II} metal ion being linked to its neighbouring metal centres Ni_{12} and Ni_{32} through HO^- groups.

3.2.3. Metal-and-Ligand-Defective Grids

Metal-and-ligand-defective grids can be generated by tri-, tetra- or pentatopic ligands.

3.2.3.1. Grids Generated by Tritopic Ligands

There are several types of grid-like complex cations: $[M_6L_5]^{x+}$, $[M_7L_5(L')_\alpha(L'')_\beta]^{x+}$ and $[M_8L_4(L')_\alpha]^{x+}$.

3.2.3.1.1. [2 × 3] Grid-Like Complex Cations $[M_6L_5]^{x+}$

In this type of grid, with respect to the complete nonanuclear one, three cations (M_{12}, M_{22}, M_{32} in the matrix-like

representation) and one ligand (L_C2, i.e. the ligand corresponding to column 2 in the matrix-like representation) are missing. There are two kinds of ligand: two columns L_C1 and L_C3 (where all tridentate sites occupied with metal ions are arranged in a more or less linear fashion), and the three rows L_R1–3 (where the central tridentate site is free). The conformations of ligands L_Cj and L_Ri are different.

3.2.3.1.1.1. Grids Generated by Tritopic py_1-$(pdz)_2$-py_1 Strands

Grid $[Ag_5(\mathbf{7a})_6]^{5+}$ (ref.[41]; Figure 19a) has been characterized by NMR spectroscopy. All bidentate sites of ligands L_Cj (j = 1, 3) are occupied and all N atoms in these ligands are in *cisoid* orientation (Figure 19b). Only the first and third sites of ligands L_Ri (i = 1, 2, 3) are occupied, and the junction between the pyridazine rings has *transoid* conformation, as in the free ligands (Figure 19c).

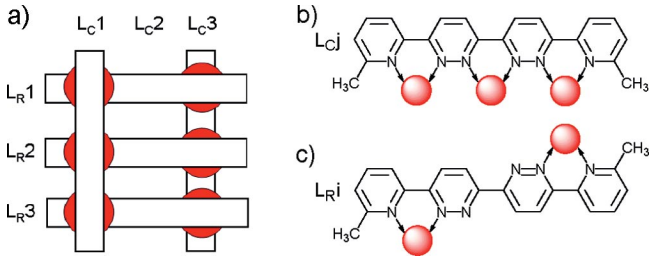

Figure 19. (a) Stylized representation of the incomplete grid $[Ag_5(\mathbf{7a})_6]^{5+}$ (ref.[41]); coordination modes of ligands L_Cj (b) and L_Ri (c) in grid $[Ag_5(\mathbf{7a})_6]^{5+}$.

3.2.3.1.1.2. Grids Generated by Tritopic py_1-$(py_2$-pym$)_2$-py_2-py_1 Strands

Incomplete [2 × 3] grids[18,19] were obtained pure or as the main product, by the reaction of ligands **8a**–**d** with various divalent metal salts, in a metal/ligand molar ratio of 3:2: $[Co_6(\mathbf{8b})_5](BF_4)_{12}$, $[Zn_6(\mathbf{8b})_5](CH_3COO)_{12}$, $[Zn_6(\mathbf{8b})_5](CF_3SO_3)_{12}$, $[Zn_6(\mathbf{8b})_5](BF_4)_{12}$, $[Co_6(\mathbf{8a})_5](CF_3SO_3)_{12}$, $[Co_6(\mathbf{8d})_5](BF_4)_{12}$, $[Fe_6(\mathbf{8d})_5](BF_4)_{12}$, $[Zn_6(\mathbf{8d})_5](BF_4)_{12}$, $[Co_6(\mathbf{8c})_5](BF_4)_{12}$, $[Fe_6(\mathbf{8c})_5](BF_4)_{12}$, $[Zn_6(\mathbf{8c})_5](BF_4)_{12}$. The counterion plays an important role in determining the nature of the grid that may form; for example, $Zn(CF_3SO_3)_2$ or $Zn(CH_3COO)_2$ reacts with **8b** and gives the [2 × 3] grid with some [2 × 2] grid as side product, while $Zn(BF_4)_2$ gives the [3 × 3] grid. The formation of the [2 × 3] grid instead of the [3 × 3] grid was explained by: (i) the pym-py_2-pym structure of the central tridentate site of ligands that renders it more poorly coordinating than the terminal pym-py_2-py_1 sites that have two pyridine groups; (ii) the fact that the binding of three cations induces curvature of the ligand and consequently strains it.

The X-ray structure of the [2 × 3] grid $[Co_6(\mathbf{8c})_5](BF_4)_{12}$ (ref.[18]; Figure 20a,d) shows that the ligand L_C2 is missing, as well as three Co^{II} cations that should have been bound to it. The external dimensions of the grid are of about 24.2 Å (the distances between the protons on the C5 atoms of terminal py_1 of ligands L_Cj) and 25 Å (the distances between the protons on the C4 atoms of py_2 of ligand L_C1 and L_C3, py_2 that belong to the same row). The grid contains two kinds of ligands: the completely occupied ones (Figure 20c), and the ones that bind only two cations and where the Nsp^2 of the central py_2 is in *s-trans* with respect to the uncoordinated Nsp^2 of the neighbouring pym rings (Figure 20b). This *transoid* conformation is found in the free ligand. π–π stacking is observed between the phenyl rings of L_Cj ligands and several pyridine and pyrimidine rings of ligands L_Ri.

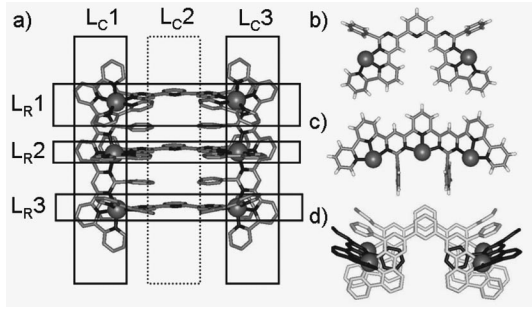

Figure 20. (a) X-ray molecular structure and matrix-like representation of grid $[Co_6(\mathbf{8c})_5]^{12+}$ (ref.[18]; the missing ligand L_C2 is shown as a rectangle with dashed lines); (b) tritopic ligand **8c** with two occupied sites; (c) tritopic ligand **8c** with three occupied sites; (d) top view of grid $[Co_6(\mathbf{8c})_5]^{12+}$.

The following [2 × 3] incomplete grids[19] were characterized by mass spectrometry: $[Cd_6(\mathbf{8b})_5](CF_3SO_3)_{12}$, $[Co_6(\mathbf{8b})_5](CF_3SO_3)_{12}$, $[Cu_6(\mathbf{8b})_5](CF_3SO_3)_{12}$, $[Pb_6(\mathbf{8b})_5](CF_3SO_3)_{12}$ (side product of $[Pb_9(\mathbf{8b})_6](CF_3SO_3)_{18}$).

3.2.3.1.1.3. Grids Generated by Bis(acylhydrazone) Ligands py_1-hyz-CO-py_2-CO-hyz-py_1

Grid-like complex $[Ni_6(\mathbf{9c}H)_5](CF_3SO_3)_7 \cdot 14H_2O$[40] (Figure 21a) is a hexanuclear [2 × 3] grid in which the five ligands $\mathbf{9c}H_2$ are half-deprotonated. Only the pseudo-octahedral cations M_{11}, M_{21}, M_{31}, M_{13}, M_{23}, M_{33} (M = Ni) are present. Row ligands L_Ri (i = 1 to 3) have one central free N_2O site and two terminal occupied N_2O sites, the two terminal sites adopting an *anti* relative orientation (Figure 21c). In column ligands L_Cj (j = 1 and 3), all three tridentate sites are occupied (Figure 21d). The average Ni–Ni distance in matrix columns is 4 Å; it is 9.3 Å in matrix rows and Ni–Ni diagonals are 11.4 and 12.6 Å. The deprotonation of the ligands occurs spontaneously, and no base was added during the preparation of the complex.

In grid-like complex $[Ni_6(\mathbf{9b})_5](BF_4)_4[Ni(H_2O)_6] \cdot 20H_2O$[40] (Figure 21b), the ligand $\mathbf{9b}H_2$ is present as its dideprotonated form $\mathbf{9b}^{2-}$ due to Et_3N addition during the preparation of the complex. In row ligands L_Ri, the two occupied tridentate sites are *syn* oriented, having two occupied N_2O sites and one free N_3 site (Figure 21e).

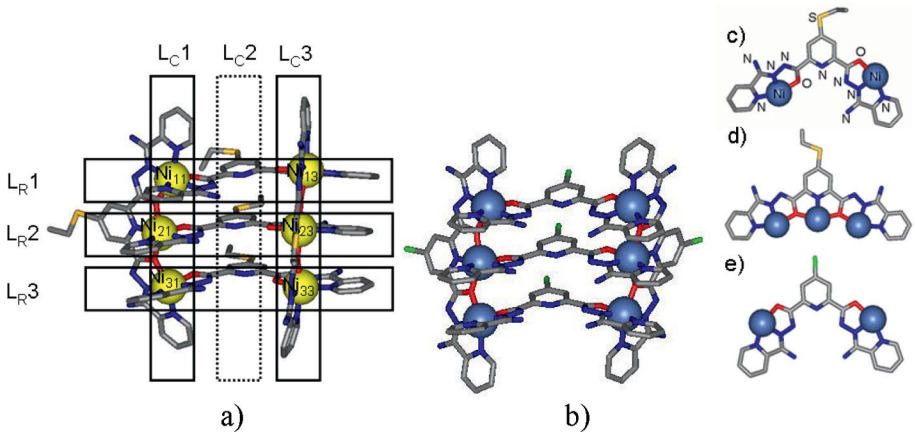

Figure 21. X-ray molecular structure of: (a) grid $[Ni_6(\mathbf{9c}H)_5]^{7+}$ (ref.[40]) superimposed on its matrix-like representation (the missing ligand L_C2 is shown as a rectangle with dashed lines), (b) grid $[Ni_6(\mathbf{9b})_5]^{2+}$ (ref.[40]; protons not shown). Coordination modes of tritopic ligands within and above the grids: (c) $\mathbf{9c}H^-$: N_2O^{occ}–N_2O^{fr}–N_2O^{occ} mode with two *anti* oriented terminal occupied sites; (d) $\mathbf{9c}H^-$: N_2O^{occ}–NO_2^{occ}–N_2O^{occ} mode with three occupied sites; (e) $\mathbf{9b}^{2-}$: N_2O^{occ}–N_3^{fr}–N_2O^{occ} mode with two *syn* oriented terminal occupied sites (occ = occupied, fr = free).

3.2.3.1.2. Complex Cation $[M_7L_5(L')_\alpha(L'')_\beta]^{x+}$

In grid-like complex $[Co^{III}_4Co^{II}_3(\mathbf{9a})_5(CH_3CN)(H_2O)_2](ClO_4)_8\cdot 4CH_3CN\cdot 9H_2O$[40] (Figure 22a), the following metal ions are present: M_{11}, M_{21}, M_{31}, M_{13}, M_{23}, M_{33}, M_{32} (M = Co). Ligand $\mathbf{9a}H_2$ is present as its dideprotonated form $\mathbf{9a}^{2-}$, but the deprotonation occurs spontaneously, no base being added during the synthesis of the complex. Co_{32} has a *mer*-N_3O_3 coordination sphere consisting of the central N_2O tridentate site of ligand L_R3, two water molecules and one acetonitrile. Ligand L_R3 is fully, but dissymmetrically occupied (Figure 22c). In row ligands, the two occupied terminal tridentate sites are *anti* oriented (Figure 22b). The average Co–Co distance in L_Cj ligands is 4 Å, while in L_R3 (Figure 22c) two very distinct Co–Co distances, 3.9 and 4.9 Å, were measured. The average Co–Co distance in ligands L_R1,2, in which the only two occupied terminal sites are *anti* oriented, is about 9.2 Å.

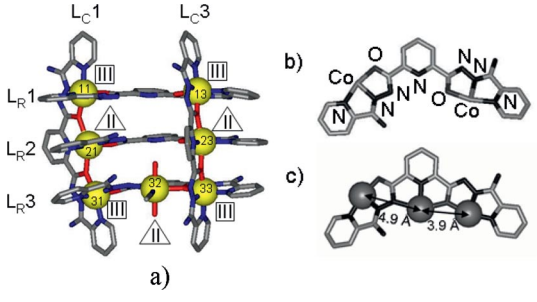

Figure 22. (a) X-ray molecular structure of grid $[Co^{III}_4Co^{II}_3(\mathbf{9a})_5(CH_3CN)(H_2O)_2]^{8+}$ (protons not shown). Co_{11}, Co_{13}, Co_{31} and Co_{33} are Co^{III}, while Co_{21}, Co_{23} and Co_{32} are Co^{II}; (b) a tridentate ligand $\mathbf{9a}^{2-}$ with two *anti* oriented occupied sites (N_2O^{occ}–N_2O^{fr}–N_2O^{occ} mode); (c) a dissymmetrically coordinated ligand $\mathbf{9a}^{2-}$ with three occupied sites and terminal sites *anti* oriented (N_2O^{occ}–N_2O^{occ}–N_2O^{occ} mode).

In this heterovalent grid, Co^{II} centres are located in positions 21, 23 and 32, while Co^{III} centres are positioned at the corners. This arrangement is to be compared with $Mn^{III}_3Mn^{II}_6$ and $Mn^{III}_4Mn^{II}_5$ [3×3] grids, where Mn^{III} ions are also positioned at the corners (vide supra).

3.2.3.1.3. Grid-Like Complexes[23,42] $[M_8L_4(L')_\alpha]^{x+}$

In this particular case, four 3-tridentate-site ligands generate "M_3L" motifs within an octanuclear architecture. The metal/ligand ratio is not 3:2 (as in a [3×3] grid), but 2:1. These octanuclear architectures have a [2×2] complete core (four metal ions) with additional external nuclearity (four metal ions), forming a "pinwheel-like" structure. The four external metal ions are coordinated only by one tridentate site of the tritopic ligand, and anions or other coordinating molecules [L′ = NO_3^-, H_2O (Figure 23d), CH_3CN; α = 8] complete their coordination environment. This kind of architecture can be described by either a 4×4 or a 2×2 matrix-like representation (Figure 23a).

In grids $[Cu_8(\mathbf{9b})_4(NO_3)_8]\cdot 20H_2O$[23] (Figure 23a) and $[Cu_8(\mathbf{9l})_4(NO_3)_8]\cdot 15H_2O$,[23] the ligands coordinate in a "normal" mode (Figure 23c), that is, there are three *syn*-oriented tridentate sites N_2O–NO_2–N_2O. Grid $[Cu_8(\mathbf{9a})_4(CH_3OH)_4(CH_3CN)_4][Gd(NO_3)_4(H_2O)_2]_2(NO_3)_6\cdot 1.3Cu(NO_3)_2\cdot 10H_2O$[42] has similar structural features, the external Cu^{II} ions having a N_3O_2 coordination sphere that includes the donor atoms from a CH_3CN and a CH_3OH molecule.

In grid $[Cu_8(\mathbf{9f})_4(H_2O)_8](ClO_4)_8$ (ref.[23]; Figure 23b), the opening of one terminal site has an orientation opposed to those of the other two sites (Figure 23d), and the central site is not a NO_2, but a N_2O site; thus the terminal sites are *anti* oriented.

As to the influence of solvent and temperature on these systems, it should be noted that both Cu^{II} octanuclear and nonanuclear ($[Cu_8(\mathbf{9b})_4(NO_3)_8]\cdot 20H_2O$ and $[Cu_9(\mathbf{9b}H)_3(\mathbf{9b})_3](NO_3)_9\cdot 20H_2O$) grids were obtained,[23] in both cases the starting salt being Cu^{II} nitrate and the metal/ligand molar ratio 3:1. The difference between their syntheses is the solvent (MeOH/MeCN, 1:1(v/v) for the octanuclear grid, and MeOH/H_2O, 1:1(v/v) for the nonanuclear grid) and the

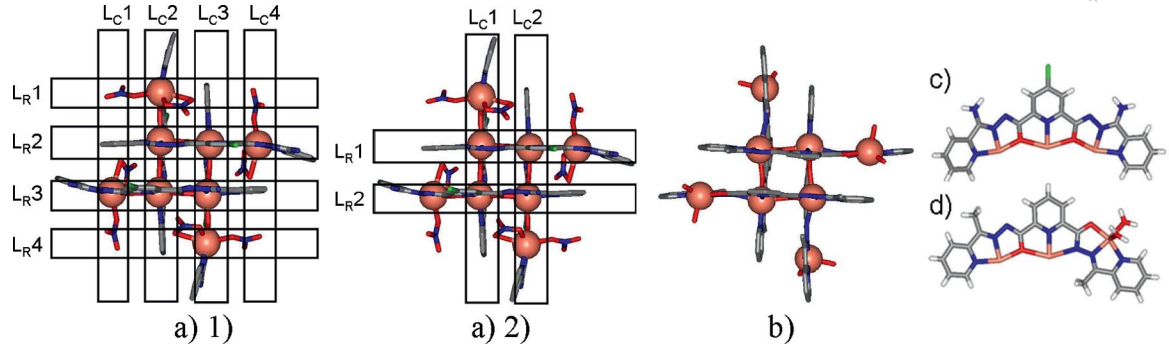

Figure 23. (a) X-ray structure and two possible matrix-like representation of grid $[Cu_8(\mathbf{9b})_4(NO_3)_8]\cdot 20H_2O$[23] (protons and water molecules not shown); (b) X-ray molecular structure of grid $[Cu_8(\mathbf{9f})_4(H_2O)_8]^{8+}$ (ref.[23]); (c) the coordination mode of ligand $\mathbf{9b}^{2-}$ (NO_3^- not shown) in grid $[Cu_8(\mathbf{9b})_4(NO_3)_8]\cdot 20H_2O$; (d) the coordination mode of ligand $\mathbf{9f}^{2-}$ in grid $[Cu_8(\mathbf{9f})_4(H_2O)_8]^{8+}$; two H_2O molecules are bound to a Cu^{II} ion.

temperature (room temperature for the octanuclear complex and warming for the nonanuclear one). The octanuclear complex can be converted into the nonanuclear one by dissolving it in MeOH/H_2O (1:1, v/v) and warming. This suggests that the nonanuclear complex is thermodynamically more favoured than the octanuclear one and shows the influence of the solvent on the nature of such metallosupramolecular architectures.

Correlatively, ligand $\mathbf{9a}H_2$ also forms an octanuclear grid $[Cu_8(\mathbf{9a})_4(CH_3OH)_4(CH_3CN)_4]^{8+}$ [from Cu^{II} nitrate, in MeOH/MeCN (2:1, v/v), metal/ligand 3:1],[42] as well as a nonanuclear one $[Cu_9(\mathbf{9a}H)_6](NO_3)_{12}\cdot 9H_2O$ (from Cu^{II} nitrate, in water, metal/ligand 6:1).[21]

Overall, it seems that polar solvents and warming stabilize nonanuclear grids, while less polar solvents and room temperature yield octanuclear grids.

3.2.3.1.4. Coordination Modes of Tritopic Bis(acylhydrazone) Ligands $9H_2$ within Ligand-and-Metal-Defective Grids

A tritopic ligand A_1-B_1-A_2-B_2-A_3-B_3-A_4 has the following coordination sites: A_1-B_1-A_2, A_2-B_2-A_3 and A_3-B_3-A_4. In the "normal" coordination mode of bis(acylhydrazone)s $\mathbf{9}H_2$ (or their mono- $\mathbf{9}H^-$ or dideprotonated form $\mathbf{9}^{2-}$), the three tridentate sites are the central NO_2 site and the two terminal N_2O sites. The simple C–C bond that links the

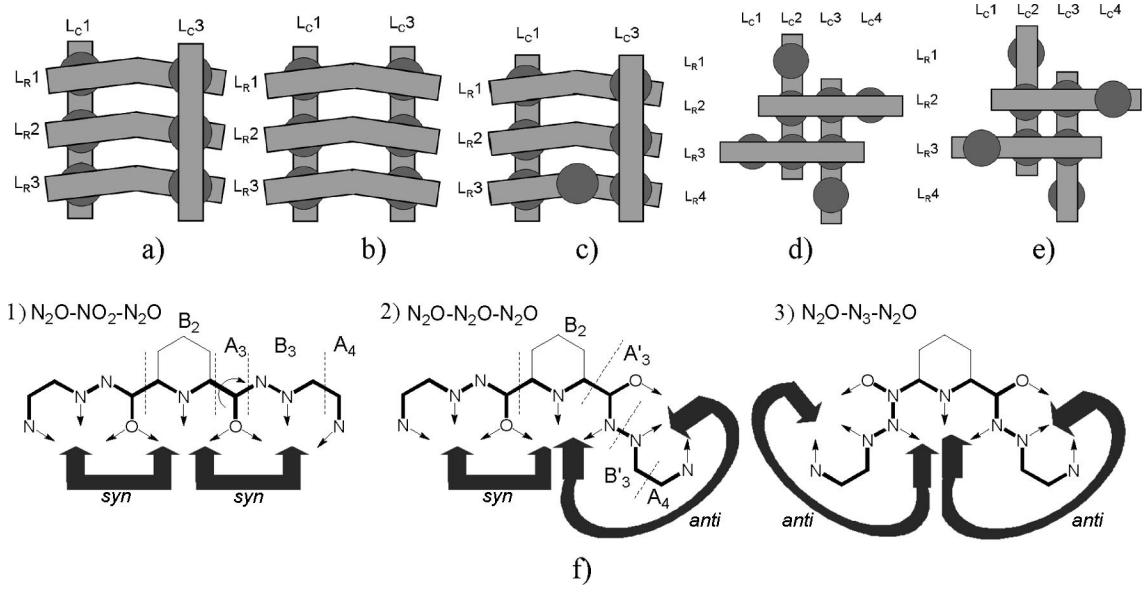

Figure 24. (a–e) Stylized representation of various types of incomplete grids generated by tritopic bis(acylhydrazone) ligands $\mathbf{9}H_2$ depending on their coordination mode (occ = occupied, fr = free): (a) L_Cj: N_2O^{occ}–NO_2^{occ}–N_2O^{occ}, L_Ri: N_2O^{occ}–N_2O^{fr}–N_2O^{occ}; (b) L_Cj: N_2O^{occ}–NO_2^{occ}–N_2O^{occ}, L_Ri: N_2O^{occ}–N_3^{fr}–N_2O^{occ}; (c) L_Cj: N_2O^{occ}–NO_2^{occ}–N_2O^{occ}, L_R1 and L_R2: N_2O^{occ}–N_2O^{fr}–N_2O^{occ}, L_R2: N_2O^{occ}–N_2O^{occ}–N_2O^{occ}; (d) L_Cj and L_Ri: N_2O^{occ}–NO_2^{occ}–N_2O^{occ}; (e) L_Cj and L_Ri: N_2O^{occ}–N_2O^{occ}–N_2O^{occ}. (f) Schematic representation of the three coordination modes and conformations of tritopic bis(acylhydrazone)s that may be described considering the relative orientation of neighbouring sites: (1) *syn-syn* corresponds to N_2O–NO_2–N_2O; (2) *syn-anti* corresponds to N_2O–N_2O–N_2O; (3) *anti-anti* corresponds to N_2O–N_3–N_2O.

–COhyz– unit to the py_2 ring may turn around its axis (as, consequently, the entire site A_1-B_1-A_2 or A_3-B_3-A_4) to generate a central N_2O tridentate site. For example, if only A_3-B_3-A_4 turns (Figure 21c, Figure 22b, Figure 23d), then A_1-B_1-A_2-B_2-A_3-B_3-A_4 becomes A_1-B_1-A_2-B_2-A'_3-B'_3-A_4. A_3 is the **CO** group and A'_3 is the **NCO** group, and B_3 is the hydrazone (N–N=CR) group, while B'_3 is N=CR group (see Figure 24f(1) and (2)). The conformational change induces a change in the nature of the coordination site.

In the sequence of coordination sites N_2O–NO_2–N_2O, the three sites have the same orientation (Figure 21d, Figure 23c, Figure 24d,f(1)), while in the sequence N_2O–N_2O–N_2O, the orientation of one terminal site is opposite to that of the other two sites. This last situation appears in many incomplete grids (Figure 21c, Figure 22b,c, Figure 23d, Figure 24a,c,e,f(2)).

When the opening of both terminal sites is opposed to the opening of the central one, then the representation of the ligand may be written A_1-B'_1-A'_2-B_2-A'_3-B'_3-A_4 and its sequence of coordinating sites is N_2O–N_3–N_2O (Figure 21e, Figure 24b,f(3)). This conformation induces, in complete grids (vide supra) that contain three N_2O–N_3–N_2O sequences and three N_2O–NO_2–N_2O sequences, an "alternate" aspect of the grid.

Another manner of describing these coordination modes is to take into account the relative orientation (*syn* or *anti*) of *neighbouring* tridentate sites, as shown in Figure 24f. There are three possible combinations *syn-syn*, *syn-anti* and *anti-anti*. Care should be taken to avoid possible confusion; for example, the *anti-anti* combination corresponds to the *syn* orientation of terminal sites.

3.2.3.2. Incomplete Grid Generated by Tetratopic Ligands

This incomplete grid,[31] obtained by reaction of ligand **11** with 3 equiv. of $Pb(CF_3SO_3)_2$ (Figure 25), belongs to the class of incomplete grids with a [2 × 2] core and external high nuclearity, that is, eight external tridentate sites able to bind eight cations. It can also be seen as a double cross.[31] In the complex cation $[Pb_{12}(\mathbf{11})_4(CF_3SO_3)_{16}(H_2O)_{10}]^{8+}$, the average Pb–Pb distance is 6.75 Å, the average distance between the C4 atoms of the terminal pyrimidines of a ligand is 29 Å and the Pb–Pb diagonals of the core [2 × 2] grid are 9.1 Å. As in the corresponding [4 × 4] grid, water molecules and triflate anions are bound to Pb^{II} metal ions.

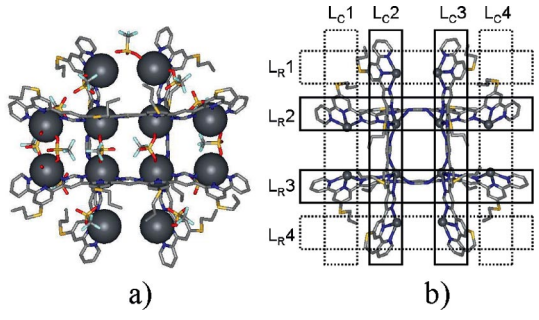

Figure 25. X-ray structure (a) and matrix-like representation (b; anions omitted) of complex $[Pb_{12}(\mathbf{11})_4(CF_3SO_3)_{16}(H_2O)_{10}]^{8+}$ (ref.[31]; protons not shown).

3.2.3.3. Incomplete Grids Generated by Five Bidentate-Site Ligands.[43]

Ligand **14** is pentatopic and was expected to generate a [5 × 5] grid with cations that adopt tetrahedral coordination geometry, such as Ag^I. Variable-temperature ^1H NMR spectroscopic studies showed that the CD_3NO_2 solution in which the $AgCF_3SO_3$/**14** molar ratio was 2.5:1 (as required to obtain grid $[Ag_{25}(\mathbf{14})_{10}]^{25+}$) contained mainly two species in slow exchange on the NMR timescale. One of these species was found to be the quadruple helicate $[Ag_{10}(\mathbf{11})_4]^{10+}$ (Figure 26d), but grids $[Ag_{25}(\mathbf{14})_{10}]^{25+}$ (the expected one) or $[Ag_{20}(\mathbf{14})_9]^{20+}$ were not observed by ^1H NMR spectroscopy. This solution gave two types of crystals: pale-yellow ones (the incomplete grid $[Ag_{20}(\mathbf{14})_9]^{20+}$, Figure 26a) and orange ones (the helicate $[Ag_{10}(\mathbf{14})_4]^{10+}$, Figure 26d).[43]

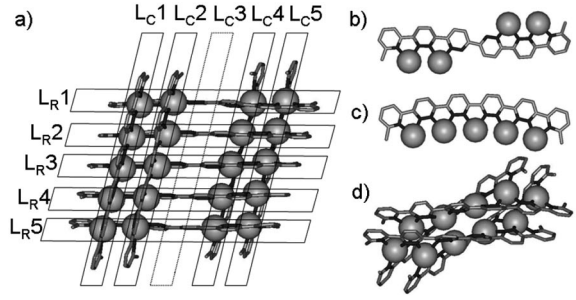

Figure 26. (a) X-ray molecular structure of grid $[Ag_{20}(\mathbf{14})_9]^{20+}$ (ref.[43]) and its matrix-like representation; (b) coordination mode of a ligand L_Ri that binds four Ag^+ ions; (c) coordination mode of a ligand L_Cj that binds five Ag^+ ions; (d) X-ray molecular structure of helicate $[Ag_{10}(\mathbf{14})_4]^{10+}$ (anions and protons not shown).

The icosanuclear incomplete grid $[Ag_{20}(\mathbf{14})_9]^{20+}$ is a [4 × 5] grid, but it can also be seen as a [2 × (2 × 5)] one, that is, as an association of two [2 × 5] sub-grids. The average distance between the protons located on C5 atoms of terminal pyridines of a ligand is 25.5 Å for ligands L_Cj that coordinate four cations and 25.1 Å for ligands L_Ri that coordinate five cations. A consequence of the coordination is that in all bidentate sites py_1-pdz and pdz-pdz that bind to a cation, the Nsp^2 atoms are in *cisoid* orientation (Figure 26c), while in the free ligand they are in *transoid* orientation. In the ligand that coordinates only four cations, the central free site has a *transoid* conformation (Figure 26b), the consequence being that the [2 × 5] sub-grids are *anti* oriented.

The preference of the [4 × 5] grid over the [5 × 5] one can be explained by the fact that the [5 × 5] one should have all Nsp^2 atoms in *cisoid* orientation, that is, 50 *cisoid* sites, while the [4 × 5] grid has only 40 *cisoid* sites. To this should be added the fact that occupation of all five sites of ligand **14** produces a curvature (Figure 26c) and consequently a strain on the ligand, as well as an increase in the volume of central coordination spheres. Moreover, if the [4 × 5] grid appeared as an intermediate during the hypothetical formation of the [5 × 5] grid, the formation of the last one would suppose a complete reorganization of the system, required in order to permit rotation around the central C_{pdz}–C_{pdz} bond.

3.3. A Pseudo-[3 × 3] Grid[44]

This is a particularly interesting case, where six ligands **16** (Figure 27a) are present and oriented like in a [3 × 3] grid, but there are four cations instead of nine (Figure 27b). Five cations are missing, not because an "unpredicted coordinative event" occurred (like for incomplete grids) even though the ligand would have been conceived to generate a [3 × 3] grid, but because the system (ligand and cations) has been designed to generate a tetranuclear [2 × 2] grid. Thanks to π–π stacking, two supplementary "guest" ligands are located between the four ligands, which, together with the four Cu^{I} ions, form the [2 × 2] grid that acts as a "host". This structural feature can be compared with the pentanuclear incomplete grid $[Fe_5(\mathbf{9a}H)_6]^{9+}$ (vide supra). From a coordinative point of view, the grid is complete. The grid has nine tetrahedral pockets, but only the four N_4 nodes corresponding to M_{11}, M_{13}, M_{31} and M_{33} are occupied with Cu^{I}. Each one of the four $(CH)_2N_2$ unoccupied pockets ($_{12}$, $_{21}$, $_{23}$ and $_{32}$) corresponds to one phenanthroline-like site and one 3,3′-bipyridine-like site. The central $(CH)_4$ unoccupied node corresponds to two 3,3′-bipyridine-like sites.

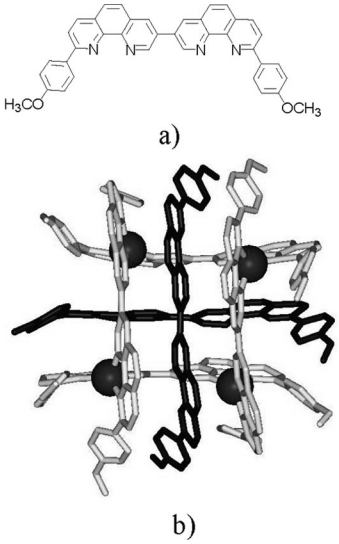

Figure 27. (a) Structural formula of ligand **16**, which generates grid $[Cu_4(\mathbf{16})_6](BF_4)_4$; (b) X-ray molecular structure of grid $[Cu_4(\mathbf{16})_6]^{4+}$ (ref.[44]; anions and protons not shown).

Despite the fact that this grid is not a grid with "unusual, high" nuclearity (as it is tetranuclear), this discussion was included here because of the similarity between this pseudo-[3 × 3] grid and a possible incomplete [3 × 3] grid, in order to better understand the difference.

4. Structural Characterization

Besides elemental analysis, infrared spectroscopy, mass spectrometry (usually electrospray mass spectrometry (ES-MS), which is a soft method of ionization) and X-ray crystallography, NMR spectroscopy and other methods were employed for the structural characterization of grids discussed in this review.

4.1. NMR Spectroscopy

Nuclear magnetic resonance spectroscopy (NMR) is a precious tool[45] of characterization.

4.1.1. ^{1}H NMR Spectroscopic Differentiation of Ligands within [3 × 3] and [4 × 4] Grids

The placement of ligands of the same kind in two different chemical environments within [3 × 3] and [4 × 4] grids makes them chemically inequivalent. Thus, the ^{1}H NMR spectra of grid $[Pb_9(\mathbf{8a})_6]^{18+}$ (not shown), as well as the one of grids $[Ag_9(\mathbf{7a})_6](CF_3SO_3)_6$[16] or $[Zn_9(\mathbf{8b})_6](BF_4)_{18}$[18] (not shown), show peaks indicating the presence of two kinds of coordinated ligands in a molar ratio of 2:1, which correspond to the outer (2 equiv.) and inner (1 equiv.) ligands. Correlatively, the ^{1}H NMR spectrum (not shown) of the [4 × 4] grid $[Pb_{16}(\mathbf{11})_8]^{32+}$ contains two sets of signals in a 1:1 ratio corresponding to two different groups of equivalent ligands: outer (L_C1, L_R1, L_C4, L_R4) and inner (L_C2, L_R2, L_C3, L_R3) (see Figure 28a).[17,31] A similar situation is observed for grid $[Pb_{16}(\mathbf{12})_8]^{32+}$ (ref.[33]; Figure 28a,b).

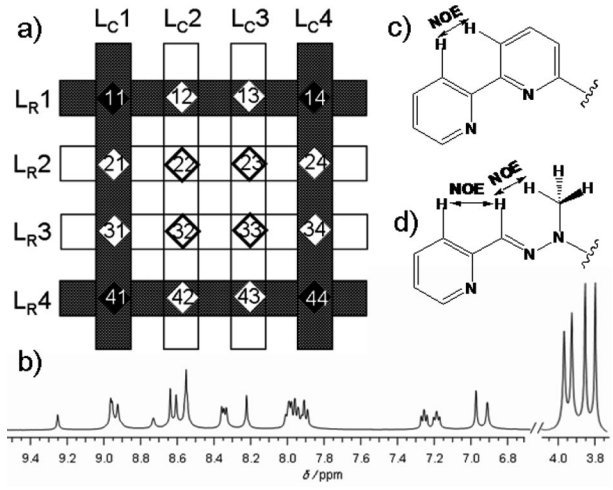

Figure 28. (a) Matrix-like representation of a [4 × 4] grid $[Pb_{16}(L)_8]^{32+}$ (L = **11**, **12**); (b) 500 MHz ^{1}H NMR spectrum[33] of the [4 × 4] grid type complex $[Pb_{16}(\mathbf{12})_8]^{32+}$ (solvent CD_3NO_2); ^{1}H–^{1}H NOE between protons of py_1-py_2 (c) or py_1-hyz (d) sequences.

In the case of grid $[Ag_6(\mathbf{7a})_3(\mathbf{4})_2]^{6+}$ (Figure 8b,c), two sets of signals in a 2:1 (outer/inner) ratio correspond to the two kinds of ligand **4** (due to the two different environments).[37]

4.1.2. Ligand Conformation in Grids – NOESY and ROESY

In ligands with coordination sites comprising two or three units that have close protons, the nuclear Overhauser effect (NOE) (Figure 28c,d) between these close protons results in ^{1}H–^{1}H correlations in the NOESY (Nuclear Overhauser Effect Spectroscopy) or ROESY (Rotating-Frame NOE Spectroscopy) spectra and thus confirms their proximity and, furthermore, the conformation of the ligands.

4.1.3. Metal Ion Differentiation Observed by NMR Spectroscopy

In the case of grid $[Pb_{16}(\mathbf{11})_8]^{32+}$ that contains three kinds of Pb^{II} (Figure 28a), that is, corner (11, 14, 41, 44), edge (21, 31, 42, 43, 24, 34) and centre (22, 23, 32, 33), the ^{207}Pb NMR spectrum contains three signals in a 1:2:1 ratio, which correspond to the three kinds of Pb^{II}.[17,31] The ^{207}Pb NMR spectrum of the double-cross-like complex $[Pb_{12}(\mathbf{11})_4]^{24+}$ contains, as expected, two signals.[31]

The ^{109}Ag NMR spectrum shows three different resonances in the expected ratios in the case of grid $[Ag_9(\mathbf{7a})_6]^{9+}$ (ref.[16]), and two signals in a 2:1 ratio in the case of grid $[Ag_6(\mathbf{7a})_2(\mathbf{4})_3]^{6+}$ (ref.[37]).

4.1.4. Proton-Metal Ion HMQC

^1H–^{207}Pb HMQC (Heteronuclear Multiple Quantum Coherence) allows identification, thanks to ^1H–^{207}Pb correlations, of the coordination sites where the cations are located. This method has particular utility when several kinds of Pb are present, as in the case of grid $[Pb_{16}(\mathbf{11})_8]^{32+}$ (ref.[31]).

4.2. Mössbauer Spectroscopy

Mössbauer spectroscopy showed that grid $[Fe^{III}{}_9(\mathbf{9a})_6](NO_3)_{15}\cdot 18H_2O$ has three kinds of cations, the intensity ratio being 1:4:4, in agreement with the three kinds of Fe^{III} in the grid (one centre, four corners, four sides).[26]

4.3. Surface Studies as a Means of Characterization – STM/CITS

Scanning tunnelling spectroscopy (STS) and current induced tunnelling spectroscopy (CITS) on highly ordered pyrolytic graphite (HOPG) or Au(111) surfaces have been performed for grids $[Mn_9\{(\mathbf{9c}H_2)_6\text{-}8H\}](ClO_4)_{10}\cdot 12H_2O$,[24,46,47] $[Mn_9(\mathbf{9b})_6](ClO_4)_6\cdot 10H_2O$[28,46,47] (Figure 29a), $[Mn_{16}(\mathbf{10b})_8(OH)_8](NO_3)_8$[28,46,47] (Figure 29b) and $[Mn_{25}(\mathbf{15}H)_{10}](ClO_4)_{20}$[28] after treatment with Et_3N (probably $[Mn_{25}(\mathbf{15})_{10}]^{10+}$) (Figure 14c). For the above $[n\times n]$ grids, CITS images show n^2 (n = 3, 4, 5) spots corresponding to the metal centres arranged as in the corresponding grid, the metal–metal separations being consistent with those measured by X-ray crystallography.

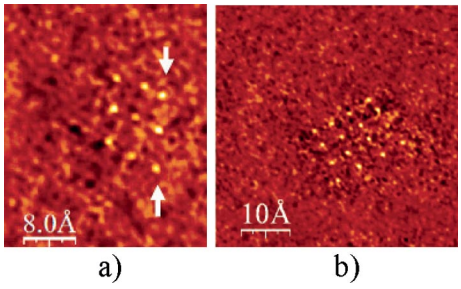

Figure 29. CITS images of grids (a) $[Mn_9(\mathbf{9b})_6](ClO_4)_6$; (b) $[Mn_{16}(\mathbf{10b})_8(OH)_8](NO_3)_8$. Reprinted with permission from ref.[28] Copyright 2007 American Chemical Society.

5. Conformational and Shape Changes of the Ligand as a Result of Coordination

The coordination of metal ions by ligands to form a grid induces conformational changes on the binding sites, whose consequence at the molecular level is the change of the shape of the ligands.

Usually, the arrangement of *s* metal ions located in the *s* sites of an *s*-topic ligand is not perfectly linear, but slightly curved.

5.1. Unbending of Bent Ligands Due to Grid Formation

Tritopic bis(acylhydrazone) ligands py_1-hyz-CO-py_2-CO-hyz-py_1 have a bent shape[51] (Figure 30a), which, on binding the amount of appropriate metal ion required to obtain the grid, is converted into a linear one (Figure 30b). For example, in the case of ligand $\mathbf{9a}H_2$, the distance between the two Nsp^3 from its NH_2 groups is about 5.5 Å in the free ligand and it increases to 12.3 Å in the ligand within the $[3\times 3]$ grid $[Zn_9(\mathbf{9a})_3(\mathbf{9a}H)_3]^{9+}$; the distance between the protons located on the C4 atoms of the terminal pyridines increases from 17 (free ligand) to 19.7 Å (grid) (Figure 30b).

5.2. Unfolding of Helical Ligands Due to Grid Formation

Ligands **11** and **12** have a defined folded helical shape that unfolds on coordination with metal ions to form the grid, thus generating an unfolding of significant amplitude.

The four-site ligand py_1-$(py_2$-pym$)_3$-py_2-py_1 (**11**) (py_1 = 2-substituted pyridine, py_2 = 2,6-disubstituted pyridine, pym = 4,6-disubstituted pyrimidine) has a helical conformation due to the *transoid* conformation of the sequences py_1-py_2 and py_2-pym.[48] The same holds for the three-site ligand py_1-$(py_2$-pym$)_2$-py_2-py_1 (**8**). The ligand py_1-(hyz-pym$)_3$-hyz-py_1 (**12**) (hyz = hydrazone), where the hyz group

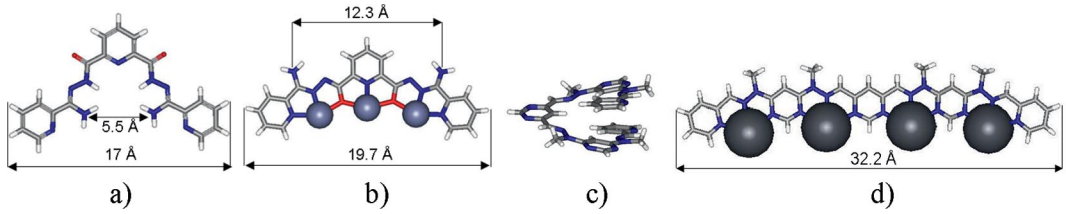

Figure 30. (a) Model of ligand $\mathbf{9a}H_2$; (b) "$Zn_3\mathbf{9a}$" motif from the $[3\times 3]$ grid $[Zn_9(\mathbf{9a})_3(\mathbf{9a}H)_3]^{9+}$; (c) helical shape of ligand **12** (X-ray structure); (d) model of a "$Pb_4\mathbf{12}$" stick of the $[4\times 4]$ grid $[Pb_{16}(\mathbf{12})_8]^{32+}$.

acts as the isomorphic equivalent of the py_2 group, also adopts a helical conformation.[49,50] In the corresponding grid-like complexes, the ligands are as their stick-like complexed form. For example, in the case of ligand **12**, the distance between the protons located on C4 atoms of terminal pyridines is 7.8 Å in the free ligand, and about 32.2 Å in the grid (Figure 29c,d).

6. Conclusion

The recent evolution of the field of grids with "unusually high" nuclearity is fast, and the grids reported until now are quite diverse. Only the aspects related to the conception and structural characteristics of such grids were reviewed here, but their very interesting properties could be discussed in a forthcoming review.

If the rational conception of *s*-site ligands often leads to the expected complete [$s \times s$] grids upon reaction with appropriate metal ions, there are also cases where an incomplete grid or another different architecture is obtained. In this process of self-assembly, the nature of the metal ion and other factors (structural strain, solvent, pH, stoichiometry etc.) play an important role.

X-ray structures of [3×3] and [4×4] complete grids were determined, and STM/CITS studies already revealed the existence of a [5×5] grid. Ligands with six and more tridentate sites were synthesized[50,52] or considered;[3a(4),3a(3)] would they lead to defined, not polymeric, complete grids? What are the limits?

In view of the recently reported heterometallic [3×3] grids, one may wonder how it would be possible to control the number of each kind of metal ion and its exact position within such grids.

Heteroleptic [2×3] grids containing two types of ligands were reported,[37a,37b] and this sparks interest for heteroleptic grids that would contain three or more types of ligand. Another interesting field would be that of grids generated by dissymmetric ligands.

To conceive the ligands and to succeed in obtaining the corresponding grids with unusual, high nuclearity is surely pure chemist-work, but it also involves a lot of know-how; it is an art.

Supporting Information (see footnote on the first page of this article): Matrix-like representation of three kinds of incomplete grids.

[1] a) J.-M. Lehn, *Supramolecular Chemistry: Concepts and Perspectives*, VCH, Weinheim, **1995**; b) M. Fujita, K. Ogura, *Coord. Chem. Rev.* **1996**, *148*, 249–264; c) P. N. W. Baxter in *Comprehensive Supramolecular Chemistry*, Vol. 9 (Eds.: J.-M. Lehn, J. L. Atwood, J. E. D. Davies, D. D. MacNicol, F. Vögtle), Pergamon, Oxford, **1996**, pp. 254–288; d) M. Fujita, *Chem. Soc. Rev.* **1998**, *27*, 417–425; e) R. V. Slone, K. D. Beckstein, S. Belanger, J. T. Hupp, I. A. Guzei, A. L. Rheingold, *Coord. Chem. Rev.* **1998**, *171*, 221–243; f) M. Fujita, *Acc. Chem. Res.* **1999**, *32*, 53–61; g) S. Leininger, B. Olenyuk, P. J. Stang, *Chem. Rev.* **2000**, *100*, 853–908; h) M. H. Keefe, K. D. Beckstein, J. T. Hupp, *Coord. Chem. Rev.* **2000**, *205*, 201–228; i) V. Balzani, A. Credi, F. M. Raymo, J. F. Stoddart, *Angew. Chem. Int. Ed.* **2000**, *39*, 3348–3391; j) S. R. Seidel, P. J. Stang, *Acc. Chem. Res.* **2002**, *35*, 972–983; k) H.-R. Tseng, S. A. Vignon, J. F. Stoddart, *Angew. Chem. Int. Ed.* **2003**, *42*, 1491–1495; l) F. Wuerthner, C.-C. You, C. R. Saha-Moeller, *Chem. Soc. Rev.* **2004**, *33*, 133–146; m) R. Dobrawa, F. Wuerthner, *J. Polym. Sci., Part A* **2005**, *43*, 4981–4995; n) M. Fujita, M. Tominaga, A. Hori, B. Therrien, *Acc. Chem. Res.* **2005**, *38*, 369–378; o) M. Schmittel, V. Kalsani, *Top. Curr. Chem.* **2005**, *245*, 1–53.

[2] See for example: a) C. Addicott, N. Das, P. J. Stang, *Inorg. Chem.* **2004**, *43*, 5335–5338; b) P. J. Stang, D. H. Cao, K. Chen, G. M. Gray, D. C. Muddiman, R. D. Smith, *J. Am. Chem. Soc.* **1997**, *119*, 5163–5168; c) P. J. Stang, B. Olenyuk, *Angew. Chem. Int. Ed. Engl.* **1996**, *35*, 732–736; d) P. J. Stang, D. H. Cao, S. Saito, A. M. Arif, *J. Am. Chem. Soc.* **1995**, *117*, 6273–6283; e) P. J. Stang, K. Chen, *J. Am. Chem. Soc.* **1995**, *117*, 1667–1668; f) A. F. Cotton, C. Lin, C. A. Murillo, *Proc. Natl. Acad. Sci. USA* **2002**, *99*, 4810–4813.

[3] a) For reviews on grid-like complexes, see: (1) L. K. Thompson, *Coord. Chem. Rev.* **2002**, *233–234*, 193–206; (2) M. Ruben, J. Rojo, F. J. Romero-Salguero, L. H. Uppadine, J.-M. Lehn, *Angew. Chem.* **2004**, *116*, 3728–3747; *Angew. Chem. Int. Ed.* **2004**, *43*, 3644–3662; (3) For the 2004 Alcan Award Lecture of L. K. Thompson that presents some of his results in high-nuclearity grid chemistry, see: L. K. Thompson, *Can. J. Chem.* **2005**, *83*, 77–92; (4) L. N. Dawe, T. S. M. Abedin, L. K. Thompson, *Dalton Trans.* **2008**, *13*, 1661–1675; (5) L. N. Dawe, K. V. Shuvaev, L. K. Thompson, *Chem. Soc. Rev.* **2009**, *38*, 2334–2359; b) For a review on two-dimensional polymers, see: J. Sakamoto, J. van Heijst, O. Lukin, A. D. Schlüter, *Angew. Chem. Int. Ed.* **2009**, *48*, 1030–1069; c) For a review on metallacrowns, see: G. Mezei, C. M. Zaleski, V. L. Pecoraro, *Chem. Rev.* **2007**, *107*, 4933–5003.

[4] a) J.-M. Lehn, *Science* **2002**, *295*, 2400–2403; b) J.-M. Lehn, *Proc. Natl. Acad. Sci. USA* **2002**, *99*, 4763–4768; c) J.-M. Lehn, *Chem. Soc. Rev.* **2007**, *36*, 151–160; d) J.-M. Lehn, *Angew. Chem. Int. Ed. Engl.* **1988**, *27*, 89–112.

[5] L. K. Thompson, O. Waldmann, Z. Xu, *Coord. Chem. Rev.* **2005**, *249*, 2677–2690.

[6] M. Ruben, J.-M. Lehn, P. Müller, *Chem. Soc. Rev.* **2006**, *35*, 1056–1067.

[7] a) R. Kieltyka, P. Englebienne, J. Fakhoury, C. Autexier, N. Moitessier, H. Sleiman, *J. Am. Chem. Soc.* **2008**, *130*, 10040–10041; b) M. L. Merlau, M. D. P. Mejia, S. T. Nguyen, J. T. Hupp, *Angew. Chem. Int. Ed.* **2001**, *40*, 4239–4242.

[8] a) B. R. Manzano, F. A. Jalón, I. M. Ortiz, M. L. Soriano, F. Gómez de la Torre, J. Elguero, M. A. Maestro, K. Mereiter, T. D. W. Claridge, *Inorg. Chem.* **2008**, *47*, 413–428; b) C. S. Campos-Fernández, R. Clérac, K. R. Dunbar, *Angew. Chem.* **1999**, *111*, 3685–3688; *Angew. Chem. Int. Ed.* **1999**, *38*, 3477–3479; c) C. S. Campos-Fernández, R. Clérac, J. M. Koomen, D. H. Russell, K. R. Dunbar, *J. Am. Chem. Soc*. **2001**, *123*, 773–774; d) C. S. Campos-Fernández, B. L. Schottel, H. T. Chifotides, J. K. Bera, J. Bacsa, J. M. Koomen, D. H. Russell, K. R. Dunbar, *J. Am. Chem. Soc*. **2005**, *127*, 12909–12923.

[9] See, for example: a) A. M. Madalan, N. Avarvari, M. Andruh, *Cryst. Grow. Des.* **2006**, *6*, 1671–1675; b) I. A. Gural′skiy, P. V. Solntsev, H. Krautscheid, K. V. Domasevitch, *Chem. Commun.* **2006**, 4808–4810; c) For porous coordination polymers generated from poly-square coordination polymers, see: K. Uemura, A. Maeda, T. K. Maji, P. Kanoo, H. Kita, *Eur. J. Inorg. Chem.* **2009**, 2329–2337.

[10] a) F. Meier, J. Levy, D. Loss, *Phys. Rev. Lett.* **2003**, *90*, 047901; b) F. Meier, J. Levy, D. Loss, *Phys. Rev. B* **2003**, *68*, 134417; c) F. Troiani, A. Ghirri, M. Affronte, S. Carretta, P. Santini, G. Amoretti, S. Piligkos, G. Timco, R. E. P. Winpenny, *Phys. Rev. Lett.* **2005**, *94*, 207–208.

[11] M. Li, P. Cai, C. Duan, F. Lu, J. Xie, Q. Meng, *Inorg. Chem.* **2004**, *43*, 5174–5176.

[12] U. Ziener, E. Breuning, J.-M. Lehn, E. Wegelius, K. Rissanen, G. Baum, D. Fenske, G. Vaughan, *Chem. Eur. J.* **2000**, *6*, 4132–4139.

[13] E. Breuning, U. Ziener, J.-M. Lehn, E. Wegelius, K. Rissanen, *Eur. J. Inorg. Chem.* **2001**, 1515–1521.
[14] M. Ruben, U. Ziener, J.-M. Lehn, V. Ksenofontov, P. Gutlich, G. B. M. Vaughan, *Chem. Eur. J.* **2005**, *11*, 94–100.
[15] For a review on nonanuclear architectures, see: A. Ruiz-Martinez, D. Casanova, S. Alvarez, *Dalton Trans.* **2008**, 2538–2583.
[16] a) P. N. W. Baxter, J.-M. Lehn, J. Fischer, M.-T. Youinou, *Angew. Chem.* **1994**, *106*, 2432–2434; *Angew. Chem. Int. Ed. Engl.* **1994**, *33*, 2284–2287; b) I. Weissbuch, P. N. W. Baxter, S. Cohen, H. Cohen, K. Kjaer, P. B. Howes, J. Als-Nielsen, G. S. Hanan, U. S. Schubert, J.-M. Lehn, L. Leiserowitz, M. Lahav, *J. Am. Chem. Soc.* **1998**, *120*, 4850–4860.
[17] A. M. Garcia, F. J. Romero-Salguero, D. Bassani, J.-M. Lehn, G. Baum, D. Fenske, *Chem. Eur. J.* **1999**, *5*, 1803–1808.
[18] E. Breuning, G. S. Hanan, F. J. Romero-Salguero, A. M. Garcia, P. N. W. Baxter, J.-M. Lehn, E. Wegelius, K. Rissanen, H. Nierengarten, A. van Dorsselaer, *Chem. Eur. J.* **2002**, *8*, 3458–3466.
[19] H. Nierengarten, E. Leize, E. Breuning, A. Garcia, F. Romero-Salguero, J. Rojo, J.-M. Lehn, A. van Dorsselaer, *J. Mass Spectrom.* **2002**, *37*, 56–62.
[20] a) A.-M. Stadler, J. Harrowfield, *Inorg. Chim. Acta* **2009**, *362*, 4298–4314 and references cited therein; b) M. Ruben, J.-M. Lehn, G. Vaughan, *Chem. Commun.* **2003**, 1338–1339; c) See for example: (1) J. Hausmann, G. B. Jameson, S. Brooker, *Chem. Commun.* **2003**, 2992–2993; (2) D. S. Cati, J. Ribas, J. Ribas-Ariño, H. Stoeckli-Evans, *Inorg. Chem.* **2004**, *43*, 1021–1030; (3) J. Klingele (née Hausmann), J. F. Boas, J. R. Pilbrow, B. Moubaraki, K. S. Murray, K. J. Berry, K. A. Hunter, G. B. Jameson, P. D. W. Boyd, S. Brooker, *Dalton Trans.* **2007**, 633–645.
[21] L. Zhao, Z. Xu, L. K. Thompson, S. L. Heath, D. O. Miller, M. Ohba, *Angew. Chem.* **2000**, *112*, 3244–3247; *Angew. Chem. Int. Ed.* **2000**, *39*, 3114–3117.
[22] L. N. Dawe, T. S. M. Abedin, T. L. Kelly, L. K. Thompson, D. O. Miller, L. Zhao, C. Wilson, M. A. Leech, J. A. K. Howard, *J. Mater. Chem.* **2006**, *16*, 2645–2659.
[23] V. A. Milway, V. Niel, T. S. M. Abedin, Z. Xu, L. K. Thompson, H. Grove, D. O. Miller, S. R. Parsons, *Inorg. Chem.* **2004**, *43*, 1874–1884.
[24] L. Zhao, Z. Xu, H. Grove, V. A. Milway, L. N. Dawe, T. S. M. Abedin, L. K. Thompson, T. L. Kelly, R. G. Harvey, D. O. Miller, L. Weeks, J. G. Shapter, K. J. Pope, *Inorg. Chem.* **2004**, *43*, 3812–3824.
[25] L. Zhao, C. J. Matthews, L. K. Thompson, S. L. Heath, *Chem. Commun.* **2000**, 265–266.
[26] L. K. Thompson, L. Zhao, Z. Xu, D. O. Miller, W. M. Reiff, *Inorg. Chem.* **2003**, *42*, 128–139.
[27] L. K. Thompson, T. L. Kelly, L. N. Dawe, H. Grove, M. T. Lemaire, J. A. K. Howard, E. C. Spencer, C. J. Matthews, S. T. Onions, S. J. Coles, P. N. Horton, M. B. Hursthouse, M. E. Light, *Inorg. Chem.* **2004**, *43*, 7605–7616.
[28] S. K. Dey, T. S. M. Abedin, L. N. Dawe, S. S. Tandon, J. L. Collins, L. K. Thompson, A. V. Postnikov, M. S. Alam, P. Müller, *Inorg. Chem.* **2007**, *46*, 7767–7781.
[29] L. N. Dawe, K. V. Shuvaev, L. K. Thompson, *Inorg. Chem.* **2009**, *48*, 3323–3341.
[30] L. Zhao, Z. Xu, L. K. Thompson, D. O. Miller, *Polyhedron* **2001**, *20*, 1359–1364.
[31] M. Barboiu, G. Vaughan, R. Graff, J.-M. Lehn, *J. Am. Chem. Soc.* **2003**, *125*, 10257–10265.
[32] S. T. Onions, A. M. Frankin, P. N. Horton, M. B. Hursthouse, C. J. Matthews, *Chem. Commun.* **2003**, 2864–2865.
[33] A.-M. Stadler, N. Kyritsakas, R. Graff, J.-M. Lehn, *Chem. Eur. J.* **2006**, *12*, 4503–4522.
[34] L. N. Dawe, L. K. Thompson, *Angew. Chem. Int. Ed.* **2007**, *46*, 7440–7444.
[35] K. V. Shuvaev, T. S. M. Abedin, C. A. McClary, L. N. Dawe, J. L. Collins, L. K. Thompson, *Dalton Trans.* **2009**, 2926–2939.
[36] L. K. Thompson, C. J. Matthews, L. Zhao, C. Wilson, M. A. Leech, J. A. K. Howard, *J. Chem. Soc., Dalton Trans.* **2001**, 2258–2262.
[37] a) P. N. W. Baxter, J.-M. Lehn, G. Baum, D. Fenske, *Angew. Chem.* **1997**, *109*, 2067–2070; *Angew. Chem. Int. Ed. Engl.* **1997**, *36*, 1978–1981; b) (1) M. Schmittel, A. Ganz, *Chem. Commun.* **1997**, 99–101; (2) M. Schmittel, U. Lüning, M. Meder, A. Ganz, C. Michel, M. Herderich, *Heterocycl. Commun.* **1997**, *3*, 493–494; (3) M. Schmittel, H. Ammon, V. Kalsani, A. Wiegrefe, C. Michel, *Chem. Commun.* **2002**, 2566–2567; (4) M. Schmittel, A. Ganz, D. Fenske, *Org. Lett.* **2002**, *4*, 2289–2292; c) M. Schmittel, V. Kalsani, D. Fenske, A. Wiegrefe, *Chem. Commun.* **2004**, 490–491; d) T. S. M. Abedin, L. K. Thompson, D. O. Miller, *Chem. Commun*. **2005**, 5512–5514.
[38] C. J. Matthews, S. T. Onions, G. Morata, M. Bosch Salvia, M. R. J. Elsegood, D. J. Price, *Chem. Commun.* **2003**, 320–321.
[39] Z. Xu, L. K. Thompson, D. O. Miller, *Polyhedron* **2002**, *21*, 1715–1720.
[40] V. Niel, V. A. Milway, L. N. Dawe, H. Grove, S. S. Tandon, T. S. M. Abedin, T. L. Kelly, E. C. Spencer, J. A. K. Howard, J. L. Collins, D. O. Miller, L. K. Thompson, *Inorg. Chem.* **2008**, *47*, 176–189.
[41] A. Marquis, J.-P. Kintzinger, R. Graff, P. N. W. Baxter, J.-M. Lehn, *Angew. Chem.* **2002**, *114*, 2884–2888; *Angew. Chem. Int. Ed.* **2002**, *41*, 2760–2764; Erratum: A. Marquis, J.-P. Kintzinger, R. Graff, P. N. W. Baxter, J.-M. Lehn, *Angew. Chem.* **2002**, *114*, 3888; *Angew. Chem. Int. Ed.* **2002**, *41*, 3738.
[42] Z. Xu, L. K. Thompson, D. O. Miller, *Chem. Commun.* **2001**, 1170–1171.
[43] P. N. W. Baxter, J.-M. Lehn, G. Baum, D. Fenske, *Chem. Eur. J.* **2000**, *6*, 4510–4517.
[44] S. Toyota, C. R. Woods, M. Benaglia, R. Haldimann, K. Wärnmark, K. Hardcastle, J. S. Siegel, *Angew. Chem.* **2001**, *113*, 773–776; *Angew. Chem. Int. Ed.* **2001**, *40*, 751–775.
[45] A. Pastor, E. Martinez-Viviente, *Coord. Chem. Rev.* **2008**, *252*, 2314–2345.
[46] J. G. Shapter, L. Weeks, L. K. Thompson, K. J. Pope, Z. Xu, M. R. Johnston, *Smart Mater. Struct.* **2006**, *15*, S171–S177.
[47] V. A. Milway, S. M. T. Abedin, V. Niel, T. L. Kelly, L. N. Dawe, S. K. Dey, D. W. Thompson, D. O. Miller, M. S. Alam, P. Müller, L. K. Thompson, *Dalton Trans.* **2006**, 2835–2851.
[48] a) G. S. Hanan, U. Schubert, D. Volkmer, E. Rivière, J.-M. Lehn, N. Kyritsakas, J. Fischer, *Can. J. Chem.* **1997**, *75*, 169–182; b) D. M. Bassani, J.-M. Lehn, G. Baum, D. Fenske, *Angew. Chem.* **1997**, *109*, 1931–1933; *Angew. Chem. Int. Ed. Engl.* **1997**, *36*, 1845–1848; c) D. M. Bassani, J.-M. Lehn, *Bull. Soc. Chim. Fr.* **1997**, *134*, 897–906; d) M. Okhita, J.-M. Lehn, G. Baum, D. Fenske, *Chem. Eur. J.* **1999**, *5*, 3471–3478.
[49] K. M. Gardinier, R. G. Khoury, J.-M. Lehn, *Chem. Eur. J.* **2000**, *6*, 4124–4131.
[50] J.-L. Schmitt, A.-M. Stadler, N. Kyritsakas, J.-M. Lehn, *Helv. Chim. Acta* **2003**, *86*, 1598–1624.
[51] The X-ray molecular structures of related compounds have been published. a) For 2,2′-bis(2-nitrobenzylidene)pyridine-2,6-dicarbohydrazide, see: B. Jia, S. Shi, F. Luo, Z. Hu, *Acta Crystallogr., Sect. E* **2006**, *62*, o3326–o3327; b) B.-M. Ji, Y.-Y. Shen, Y.-J. Wu, K.-L. Ding, S.-Q. Huo, *Jiegou Huaxue* **1998**, *17*, 319–324; c) For *N2*,*N2′*-bis[2-(ethoxycarbonylmethoxy) benzylidene]pyridine-2,6-dicarbohydrazide, see: F. Luo, S. Lan, C. Cheng, Z. Hu, *Acta Crystallogr., Sect. E* **2008**, *64*, o185; d) Y. Zhao, B. Zhang, C. Duan, Z. Lin, Q. Meng, *New J. Chem.* **2006**, *30*, 1207–1213.
[52] a) D. M. Bassani, J.-M. Lehn, *Bull. Soc. Chim. Fr.* **1997**, *134*, 897–906; b) D. M. Bassani, J.-M. Lehn, G. Baum, D. Fenske, *Angew. Chem.* **1997**, *109*, 1931–1933; *Angew. Chem. Int. Ed. Engl.* **1997**, *36*, 1845–1848; c) M. Ohkita, J.-M. Lehn, G. Baum, D. Fenske, *Chem. Eur. J.* **1999**, *5*, 3471–3481.

Received: August 4, 2009
Published Online: October 27, 2009

